

# Syneruptive incorporation of martian surface sulphur in the nakhlite lava flows revealed by S and Os isotopes and highly siderophile elements: implication for mantle sources in Mars

N. Mari<sup>a,\*</sup>, A.J.V. Riches<sup>b</sup>, L.J. Hallis<sup>a</sup>, Y. Marrocchi<sup>c</sup>, J. Villeneuve<sup>c</sup>,  
P. Gleissner<sup>d</sup>, H. Becker<sup>d</sup>, M.R. Lee<sup>a</sup>

<sup>a</sup> School of Geographical and Earth Sciences, University of Glasgow, University Avenue, Glasgow G12 8QQ, UK

<sup>b</sup> Department of Earth Sciences, Durham University, Stockton Road, Durham DH1 3LE, UK

<sup>c</sup> Centre de Recherches Pétrographiques et Géochimiques, CNRS, Université de Lorraine, UMR 7358, Vandoeuvre-lès-Nancy 54501, France

<sup>d</sup> Freie Universität Berlin, Institut für Geologische Wissenschaften, Kaiserswerther Str. 16-18, 14195 Berlin, Germany

Received 30 November 2018; accepted in revised form 17 May 2019; available online 24 May 2019

## Abstract

Martian lava flows likely acquired S-rich material from the regolith during their emplacement on the planet's surface. We investigated five of the twenty known nakhlites (Nakhla, Lafayette, Miller Range (MIL) 090032, Yamato 000593, and Yamato 000749) to determine whether these lavas show evidence of regolith assimilation, and to constrain the potential implications that this process has on chemical tracing of martian mantle source(s). To establish the proportionate influence of atmospheric, hydrothermal, and volcanic processes on nakhlite isotopic systematics we obtained *in situ* sulphur isotope data ( $\Delta^{33}\text{S}$  and  $\delta^{34}\text{S}$ ) for sulphide grains (pyrrhotite and pyrite) in all five nakhlite samples. For Nakhla, Lafayette, and MIL 090032, these data are integrated with highly siderophile element (HSE) abundances and Os-isotope compositions, as well as textural information constrained prior to isotopic analysis. This work thereby provides the first Re-Os isotope systematics for two different nakhlites, and also the first Re-Os isotope data for martian sample for which detailed petrographic information was constrained prior to digestion.

We report the largest variation in  $\delta^{34}\text{S}$  yet found in martian meteorites ( $-13.20\text{‰}$  to  $+15.16\text{‰}$ ). The relatively positive  $\Delta^{33}\text{S}$  and  $\delta^{34}\text{S}$  values of MIL 090032 ( $\delta^{34}\text{S} = +10.54 \pm 0.09\text{‰}$ ;  $\Delta^{33}\text{S} = -0.67 \pm 0.10\text{‰}$ ) indicate this meteorite assimilated sulphur affected by UV-photochemistry. In contrast, the strongly negative values of Lafayette ( $\delta^{34}\text{S} = -10.76 \pm 0.14\text{‰}$ ;  $\Delta^{33}\text{S} = -0.09 \pm 0.12\text{‰}$ ) are indicative of hydrothermal processes on Mars. Nakhla, Yamato 000593, and Yamato 000749 sulphides have a narrower range of sulphur isotope compositions ( $\Delta^{33}\text{S}$  and  $\delta^{34}\text{S} \sim 0$ ) that is consistent with no assimilation of martian surface materials during lava flow emplacement. Consequently we used this second group of  $\Delta^{33}\text{S}$  values to approximate the  $\Delta^{33}\text{S}$  of the nakhlite source, yielding a  $\Delta^{33}\text{S}$  value of  $-0.1\text{‰}$ .

Nakhlite HSE patterns result from a sulphide-saturated melt where Ru-Os-Ir alloys/sulphide were likely crystallized during earlier phases of magmatic processing in Mars to result in the fractionated HSE patterns of the nakhlites. Our data, alongside a synthesis of previously published data, suggest assimilation of an enriched component to the primary nakhlite melt, potentially a late-stage crystallization cumulate from the martian magma ocean stage. In the context of this model, and within large

\* Corresponding author.

E-mail address: [n.mari.1@research.gla.ac.uk](mailto:n.mari.1@research.gla.ac.uk) (N. Mari).

uncertainties, our data hint at perturbation and potential decoupling of nakhlite Re-Os isotope systematics from other isotopic systems as a result of small degrees of assimilation of a regolith component with highly radiogenic  $^{187}\text{Os}/^{188}\text{Os}$ .

© 2019 The Author(s). Published by Elsevier Ltd. This is an open access article under the CC BY license (<http://creativecommons.org/licenses/by/4.0/>).

**Keywords:** Mars; nakhlites; S isotopes; Os isotopes; planetary geochemistry; martian volcanism; early planetary differentiation

## 1. INTRODUCTION

Magma represent windows to comprehend the interior evolution and geochemical diversity of terrestrial planets. Magmatic activity and degassing are key processes for transferring sulphur, along with other elements, from the interior to the surface during the evolution of a planetary body. In the case of Mars, low water activity, low temperatures, and the lack of plate tectonics has favoured the preservation of a sulphur-rich regolith during the last  $\sim 2$  billion years (King and McLennan, 2010). In fact, the martian regolith contains concentrations of  $\text{SO}_2$  up to 8 wt.% (Clark et al., 1976; Foley et al., 2003).

The terrestrial and martian mantles have been reported to contain similar and chondrite-relative highly siderophile elements (HSE; Os, Ir, Ru, Rh, Pt, Pd, Au, and Re) abundances (Birck and Allegre, 1994; Warren and Kallemeyn, 1996; Brandon et al., 2000, 2012; Dale et al., 2012; Tait and Day, 2018), which has important implications for accretion theory and astrophysical modelling of Solar System evolution (e.g., Bottke et al., 2010). However, sulphur abundance estimates for the martian mantle range between 400 and 2200 ppm (Wang and Becker, 2017 and references therein) – much higher than the Earth's mantle (around 250 ppm; McDonough and Sun, 1995). The aim of this study was to use rhenium-osmium (Re-Os) isotope systematics and HSE abundances, alongside S-isotope systematics, to test whether the nakhlite group of martian meteorites preserve robust isotopic information from the martian interior (Morgan, 1986; Shirey and Walker, 1998; Righter et al., 2000; McSween and Huss, 2010; Walker, 2016).

Martian meteorites are the only available rocks from the surface of Mars. These meteorites can be divided into shergottites (basalts), nakhlites (clinopyroxene-rich rocks), and chassignites (olivine cumulates), with a few other exceptional meteorites. Berkley et al. (1980), Treiman (1986, 2005), and Bridges and Grady (2000) argued that nakhlite petrographic features are consistent with this suite of meteorites sampling a single cumulate pile. However, recent  $^{40}\text{Ar}$ - $^{39}\text{Ar}$  geochronology suggests that their crystallization ages differ by  $\sim 93$  Ma, consistent with the nakhlites being derived from a series of lava flows or sills that were emplaced between  $\sim 1416$  and  $1322$  Ma, probably from the same source (Cohen et al., 2017; Udry and Day, 2018). In this manuscript, we refer to the nakhlites as a series of lava flows.

Franz et al. (2014) used a combination of bulk rock sulphur analyses ( $\delta^{34}\text{S}$ ,  $\Delta^{33}\text{S}$ ,  $\Delta^{36}\text{S}$ ) and *in situ* pyrrhotite mineral analyses ( $\delta^{34}\text{S}$ ,  $\Delta^{33}\text{S}$ ) to determine sulphur isotope anomalies in martian meteorites. These authors determined the  $\Delta^{33}\text{S}$  of the shergottite mantle source to be  $0.009\text{‰}$ , based on the mean value of 28 meteorites. This value closely

corresponds to the value measured for the shergottite Yamato (Y)-980459, which reportedly retains the most reliable signatures of the martian mantle (e.g., Usui et al., 2012). However, Franz et al. (2014) were unable to calculate a robust value for the nakhlite mantle source region, as *in situ* secondary ion mass spectrometry (SIMS) analyses of sulphide grains were acquired from only two of the nakhlites (Nakhla and Miller Range (MIL) 03346) and their  $\Delta^{33}\text{S}$  values varied widely ( $0.06 \pm 0.21\text{‰}$  and  $-0.72 \pm 0.13\text{‰}$ , respectively). This variation was reported to have been caused by sulphate assimilation during melt eruption, affecting subsequent pyrrhotite crystallization. Franz et al. (2014) argued that sulphides and sulphates in the martian meteorites can thus be affected by assimilation of sulphur derived from atmospheric UV photochemical reactions, which was deposited at the surface as oxidized sulphur and incorporated in the martian regolith. This data is in agreement with other previously published sulphur isotope data for the nakhlites, including evidence for mass independent fractionation (MIF), which suggests assimilation of sulphur occurred at some point during nakhlite formation (e.g., Farquhar et al., 2000, 2007; Greenwood et al., 2000a,b; Dottin III et al., 2018).

These sulphur isotope systematics can be used to discern if the HSE abundances in nakhlite magmas are affected by crustal assimilation, or if they represent Mars mantle reservoirs. The HSE systematics of martian meteorites have been used to infer chondritic relative abundances of these elements in the martian mantle, and to thereby trace late-accretion of broadly chondritic materials to Mars after the last major magma ocean phase at  $\sim 4.5$  Ga (e.g., Brandon et al., 2000, 2012; Riches et al., 2011; Tait and Day, 2018). Crucially, the HSEs exhibit chalcophile element behaviour when metal is absent from the mineralogical assemblage, preferring to partition into sulphides (Day et al., 2016, and references therein), which is important in terms of HSE partitioning.

Rhenium-Os isotope data are available for many shergottites and one chassignite, but with respect to the nakhlite meteorites there are only two analyses of Nakhla (Brandon et al., 2000; Dale et al., 2012). This lack of published data is, in part, due to the low abundance of HSE ( $0.1$ – $2$  ppb or less) in the nakhlites (Treiman, 1986; Jones et al., 2003). In addition, a large age correction needs to be applied ( $1.3$  Ga since nakhlite crystallization), and the effects of crustal assimilation within Nakhla are not clear (McCubbin et al., 2013; Franz et al., 2014; Udry and Day, 2018). Therefore, Nakhla may not be a reliable indicator of the nakhlite's true Os-isotopic mantle source composition. To address these challenges, we have expanded the nakhlite Re-Os isotope and HSE dataset to include Lafayette and one of the paired Miller Range nakhlites (MIL

090032). These two meteorites are potentially highly informative as they plot at the two extremes of S-isotope composition for the nakhlites (Farquhar et al., 2000; Greenwood et al., 2000a,b; Franz et al., 2014). We also analysed a fraction of Nakhla. This nakhlite is known to have S-isotope composition of aggregated sulphides intermediate to the Miller Range and Lafayette meteorites. Sulphur isotope ( $\Delta^{33}\text{S}$  and  $\delta^{34}\text{S}$ ) data were acquired from sulphide grains in Nakhla, Lafayette, MIL 090032, Y-000749, and Y-000593 to determine the amount of crustal assimilation that has occurred in each meteorite during eruption, and to define the possible  $\Delta^{33}\text{S}$  range for the nakhlite mantle source.

## 2. METHODOLOGY

### 2.1. Sample preparation and chemical mapping

Chips were used for Re-Os isotope and HSE analysis, while thin sections were used for S-isotope analyses. The chips ( $\sim 0.5$  g) were from Nakhla (BM.191325), Lafayette (BM.1979755), and MIL 090032 (100); thin sections were from Nakhla (BM.191326#2), Lafayette (BM.1979755), MIL 090032 (28), Y-000593 (37), and Y-000749 (59). Samples were obtained from the Natural History Museum of London (Nakhla, Lafayette), NASA Johnson Space Center (MIL 090032), and JAXA (Y-000593, Y-000749). All samples were from the interior portions of the meteorite, lacking any fusion crust.

We used a novel methodology in which petrographic information was constrained, for the first time, prior to destruction of that same sample volume via acid digestion. This approach provides mineralogical context to inform our interpretations of HSE-abundance and Re-Os isotopic data. To achieve this, we polished the sample chips of Nakhla (0.4 g) and Lafayette (0.6 g) using disks of SiC and  $0.3\ \mu\text{m}$  of  $\text{Al}_2\text{O}_3$ , then rinsed with MQ  $\text{H}_2\text{O}$ . The procedure was undertaken to remove any potential contamination to the chips' surface from earlier cutting and processing by the meteorite curators. As the final step of this treatment involved repeated rinsing in MQ  $\text{H}_2\text{O}$  and visual inspection, we believe that any potential contamination of the sample by  $\text{Al}_2\text{O}_3$  residue was removed. However, it remains possible that microscopic traces of  $\text{Al}_2\text{O}_3$  could introduce Re, very small amounts of radiogenic Os, and potentially perturb the HSE and Os isotopic systematics, in which case we would anticipate variable chondrite-relative HSE patterns for the analysed nakhlites. The MIL 090032 chip (0.5 g) had a flat surface and did not require polishing. These chips were not subject to carbon coating during the acquisition of high spatial resolution images and compositional mapping. Corresponding thin sections for each of the nakhlites used in this work were carbon coated to a thickness of 20–25 nm for compositional mapping by secondary electron microscopy prior to ion microprobe work.

A Zeiss field-emission Scanning Electron Microscope (SEM), housed in the Imaging Spectroscopy and Analysis Centre of the University of Glasgow, was used to characterise thin-sections and the flat side of the prepared chips. Operating conditions were: 8.5 mm working distance,

2.15 nA beam current, and 20 kV accelerating voltage. Acquired X-ray spectra were calibrated using mineral standards. Backscattered electron (BSE) images and energy dispersive spectroscopy (EDS) X-ray element maps (for Si, Mg, Fe, Ca) were obtained for the chips lacking carbon coating with the SEM operated in low vacuum. Backscattered electron images and EDS X-ray spectra were generated for carbon coated thin sections of Nakhla, Lafayette, MIL 090032, Y-000749, and Y-000593 with the SEM operated at high vacuum. Of particular interest were the sulphides (pyrrhotite/pyrite). Every recognized sulphide on the exposed surface was imaged and quantitatively chemically analysed to determine its mineralogy (see [Supplementary Materials](#) for further details).

### 2.2. Sulphur isotope systematics

To obtain the desired spatial resolution during *in situ* analysis of pyrrhotite and pyrite for  $\delta^{34}\text{S}$ ,  $\delta^{33}\text{S}$ , and  $\Delta^{33}\text{S}$ , five polished thin-sections (one each of Nakhla, Lafayette, MIL 090032, Y-000749, and Y-000593) were analysed via SIMS. Samples were cleaned with ethanol and coated with gold to a thickness of  $\sim 20\ \mu\text{m}$ , to permit conductivity, before loading into the sample chamber of the ion probe.

Sulphur isotope compositions were measured on the CAMECA IMS 1280 ion microprobe (SIMS) at the Centre de Recherches Pétrographiques et Géochimiques (CRPG) in Nancy (France) by simultaneous measurements of  $^{32}\text{S}^-$ ,  $^{33}\text{S}^-$ , and  $^{34}\text{S}^-$  in multicollection mode with three off-axis Faraday cups (FCs) in slit 2 mode that allows for a mass resolution  $M/\Delta M = 5000$ . The FCs were intercalibrated before the analytical session to determine their relative yields. Samples were sputtered with a  $\text{Cs}^+$  primary beam of 3-nA intensity, accelerated at 13 kV and focused on a spot of  $\sim 15\ \mu\text{m}$  diameter. Pyrite, pyrrhotite and galena standards were used to determine the instrumental mass fractionation (IMF) and the reference mass instrumental law (allowing  $\Delta^{33}\text{S}$  to be calculated). Typical  $^{32}\text{S}$  count rates were between  $\sim 1.2 \times 10^9$  and  $1.5 \times 10^9$  cps, depending on the sulphide standard analysed. A typical analysis consisted of 2 min of pre-sputtering with a  $20\ \mu\text{m}$  raster, followed by data acquisition for 40 cycles of 5 s each. Faraday cup backgrounds were measured during the pre-sputtering before each analysis and then used for correcting the data. Automatic mass and transfer deflector centerings were implemented in the analysis routine to ensure reproducible analytical conditions during the session. Each measurement takes around 7 min per spot. Typical  $\pm 2\sigma$  standard errors achieved under these conditions were  $\sim 0.1$ – $0.3\text{‰}$  for  $\delta^{34}\text{S}$ ,  $\sim 0.1$ – $0.2\text{‰}$  for  $\delta^{33}\text{S}$ , and  $\sim 0.1$ – $0.25\text{‰}$  for  $\Delta^{33}\text{S}$ .

### 2.3. Analytical procedure for Os-isotope systematics and HSE

Nakhla, Lafayette, and MIL 090032 were analysed for HSE abundances and Re-Os isotope compositions. Textural characterisation of each sample fragment was retained prior to destruction of the same material fraction. All samples were weighed before and after crushing so that any loss of sample during this process could be quantified. The HSE

chemical separation for Nakhla and Lafayette was conducted in ultra-clean laboratories at the Durham Geochemistry Centre (class 100), Durham University (see [Supplementary Materials](#) for further details). We used a mixed  $^{190}\text{Os}$ – $^{191}\text{Ir}$ – $^{99}\text{Ru}$ – $^{194}\text{Pt}$ – $^{106}\text{Pd}$ – $^{185}\text{Re}$  basalt spike for Nakhla and Lafayette. This spike was selected because we anticipated fractionated HSE in the nakhlites relative to chondrite or peridotite-like HSE abundances; the basalt spike has high Re/Os thereby ensuring accurate spiking. The Total Procedural Blank (TPB) and sample digestions were processed in a high pressure asher and run at 270 °C for 18 h to liberate the HSE from sample powders and to achieve sample-spike equilibration. Following this digestion step, extraction of Os from the solution was performed using a chloroform solvent extraction approach (after [Cohen and Waters, 1996](#)). Osmium was then back-extracted into HBr, and was purified via microdistillation ([Birck et al., 1997](#)) prior to filament loading. All the other analysed HSE were separated and purified using anion exchange and LN-spec chromatography (cf., [Pearson and Woodland, 2000](#); [Puchtel et al., 2008](#); [Chu et al., 2015](#); [Supplementary Materials](#)).

MIL 090032 was analysed in the laboratories at the Freie Universität Berlin following similar laboratory processing protocols to those of Durham University. The polished surface of the sample chip was cleaned with some ethanol but not further abraded because the surface appeared porous and the chip fragile. Afterwards the chip was powdered in an agate mill. Sample digestion and chemical separation was conducted following the protocol of [Fischer-Gödde et al. \(2010, 2011\)](#). To remove Zr an additional clean-up step was applied for Pd following the protocol of [Chu et al. \(2015\)](#). Acquisition of  $^{187}\text{Os}/^{188}\text{Os}$  for this one sample fragment was unsuccessful.

The HSE were measured using an Element XR instrument (Berlin) and Element 2 (Durham). The sample was introduced via a conventional Scott-type glass spray chamber. An Aridus I membrane desolvation system was used for HSE at Berlin. Highly siderophile element signals were detected in low resolution mode with a secondary electron multiplier. Rubidium, Sr, Y, Zr, Mo, Cd, Tm, Yb, Lu, Hf, Ta, Os, and Hg were analyzed to monitor isobaric interferences and potentially interfering oxide species. Oxide formation rates were <4.5% and <0.8% for the Scott-type spray chamber at Berlin and Durham, respectively, and <0.15% using the Aridus at Berlin. The internal precision of measured isotope ratios ranges from 0.2 to 0.8% (2 $\sigma$ ). Background-corrected element ratios were corrected for mass discrimination using IUPAC values by comparison with ratios in a HSE standard solution measured in the same sequence. Isotopic ratios of  $^{99}\text{Ru}/^{101}\text{Ru}$ ,  $^{105}\text{Pd}/^{108}\text{Pd}$ ,  $^{185}\text{Re}/^{187}\text{Re}$ ,  $^{191}\text{Ir}/^{193}\text{Ir}$  and  $^{194}\text{Pt}/^{195}\text{Pt}$  were used for isotope dilution calculations. Isotope ratios  $^{105}\text{Pd}/^{106}\text{Pd}$  and  $^{194}\text{Pt}/^{196}\text{Pt}$  were used to monitor possible interferences. Concentrations of monoisotopic Rh and Au were determined via a combined internal/external standardization technique for the  $^{197}\text{Au}/^{191}\text{Ir}$  and  $^{103}\text{Rh}/^{101}\text{Ru}$  ratios ([Fischer-Gödde et al., 2010](#)). Consistency and possible interferences were checked by comparison to results from  $^{197}\text{Au}/^{195}\text{Pt}$  and  $^{103}\text{Rh}/^{191}\text{Ir}$  ratios. Four blanks were deter-

mined. Blank contributions are: 8.4% Re; 24% Ir; 3.8% Ru; 1.1% Pt; 2.9% Rh; 17.5% Pd; 24% Au at Berlin; while blank contributions at Durham are Re, 0.42–0.49%; Os, 0.70–4.20%,  $^{187}\text{Os}/^{188}\text{Os} = 0.132$ ; Ir, 0.10–0.26%; Ru, 0.04%; Pt, 0.25–0.4%; Pd, 0.87–1.0%. The elemental abundances of the samples were corrected using the blank values reported in the [Supplementary Materials](#).

### 3. RESULTS

#### 3.1. Textural characterization of the chips

The Nakhla chip ([Fig. 1a](#)) was characterized by a high proportion of mostly euhedral augite (~80%; 1–1.5 mm), and a lesser volume of euhedral to subhedral olivine (~8%; 0.3–1 mm in maximum dimension) – extensive areas of the chip had no olivine crystals. Plagioclase made up ~5 vol.% of the sample, while mesostasis represented ~7 vol.%. Texturally, a low degree (<10%) of fracturing was observed among the minerals. A single 0.3 mm long sulphate grain was present in a Si-rich area of the chip ([Fig. 1a](#)). Other smaller (<0.1 mm) sulphates and sulphides were present throughout the chip.

The Lafayette chip ([Fig. 1b](#)) was characterized by a higher proportion of euhedral to subhedral olivine (~15%; 200–800  $\mu\text{m}$  crystal size) and a lower volumetric percentage of pyroxene (~75%; 500–1800  $\mu\text{m}$  in maximum dimension) relative to the Nakhla chip; mesostasis was ~10 vol.%. Pyroxene was mostly subhedral and in some cases contained olivine inclusions of <50  $\mu\text{m}$ . The chip was characterized by a low degree (<10%) of mineral fracturing and several small (<0.1 mm) sulphates and sulphides.

The MIL 090032 chip ([Fig. 1c](#)) was characterized by a high proportion of mostly euhedral pyroxene (~80%; 1000–1300  $\mu\text{m}$  crystal sizes), with a minor amount of olivine (~10%; generally 500–700  $\mu\text{m}$  in maximum dimension) and a magnetite/olivine-rich mesostasis (~10%) that contains numerous microcrystals (<5  $\mu\text{m}$ ) of olivine. The chip shows a low degree (<15%) of fracturing. In some areas, both olivine and pyroxene contained glassy inclusions of 30  $\mu\text{m}$  in maximum dimension. Olivine was distributed heterogeneously and it occurred only in one area.

Our observations of these nakhlite chips are in agreement with previous petrographic observations of thin sections and chips of Nakhla ([Treiman, 1990](#); [Lentz et al., 1999](#); [Corrigan et al., 2015](#); [Udry and Day, 2018](#)), Lafayette ([Bunch and Reid, 1975](#); [Boctor et al., 1976](#); [Treiman et al., 1993](#); [Corrigan et al., 2015](#); [Udry and Day, 2018](#)), and MIL 090032 ([Day et al., 2005, 2006](#); [Stopar et al., 2005](#); [Udry et al., 2012](#); [Corrigan et al., 2015](#); [Udry and Day, 2018](#)). However, the Nakhla chip studied here differs from previous observations in hosting a large sulphate grain, supporting heterogeneously distributed HSE-carrying trace phases in nakhlites.

#### 3.2. Sulphur isotopes

Pyrrhotite and pyrite grains were identified adjacent to mesostasis (glass) in each thin section, and also occur as inclusions within augite ([Fig. 2](#)). These sulphides differ in



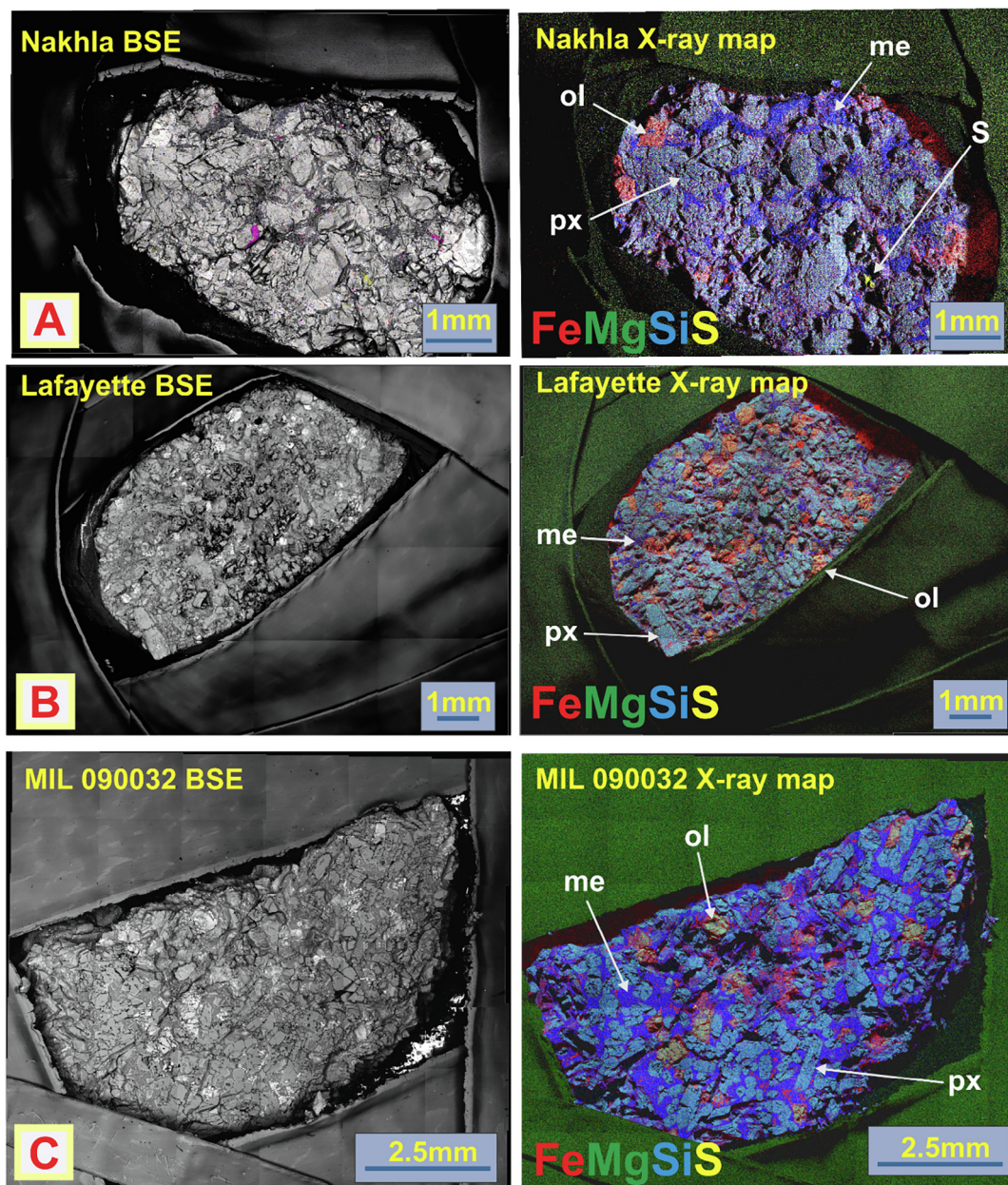


Fig. 1. Backscatter electron (BSE) images, along with false-colour Fe-Mg-Si-S X-ray elemental maps of the nakhlite chips used to retain information on the crystallographic features of our samples prior to destructive analyses for HSE abundances and Os isotopic compositions. The colour-coded elemental key is given at the bottom left of each X-ray image – olivine appears green to red, sulphide/sulphate appears yellow, clinopyroxene appears cyan, and mesostasis appears dark blue. (a) BSE image and X-ray map of Nakhla. In both images a 0.3 mm long sulphate is evident at the bottom right corner, and salt is highlighted in purple in the BSE image; (b) BSE image and X-ray map of Lafayette; (c) BSE image and X-ray map of MIL 090032. Ol, olivine; px, pyroxene; s, sulphate; me, mesostasis. (For interpretation of the references to colour in this figure legend, the reader is referred to the web version of this article.)

size between meteorites: Nakhla 20–40  $\mu\text{m}$ ; Lafayette 20–60  $\mu\text{m}$ ; MIL 090032 10–60  $\mu\text{m}$ ; Y-000593 50–250  $\mu\text{m}$ ; and Y-000749 15–40  $\mu\text{m}$ . The sulphide grains are relatively pure, containing few inclusions, or exsolved blebs/lamellae, of other phases. Sulphides in the five nakhlites analysed here show significant variation in sulphur isotopic composition, with  $\Delta^{33}\text{S}$  from  $-0.76$  to  $0.04\text{‰}$  and  $\delta^{34}\text{S}$  from  $-13.2$  to  $15.1\text{‰}$  (Table 1). Sulphur isotopes analysed from five pyrrhotite grains in Nakhla give a range of  $\Delta^{33}\text{S}$  from

$-0.12$  to  $0.02\text{‰}$ , with an average of  $-0.05 \pm 0.08\text{‰}$  and an average  $\delta^{34}\text{S}$  of  $-1.59 \pm 0.10\text{‰}$ . These values are in agreement with  $\Delta^{33}\text{S} = -0.09\text{‰}$  analysed via acid extraction and with  $\delta^{34}\text{S}$  of  $-1.6\text{‰}$  analysed via chrome reducible sulphur extraction in sulphides from Nakhla by Farquhar et al. (2007). However, our data show a slightly more negative result relative to the data of Franz et al. (2014) (mean  $\Delta^{33}\text{S} = 0.08\text{‰}$  with some grains as low as  $-0.33\text{‰}$ , and mean  $\delta^{34}\text{S} = -0.51\text{‰}$ . The SIMS measurements of

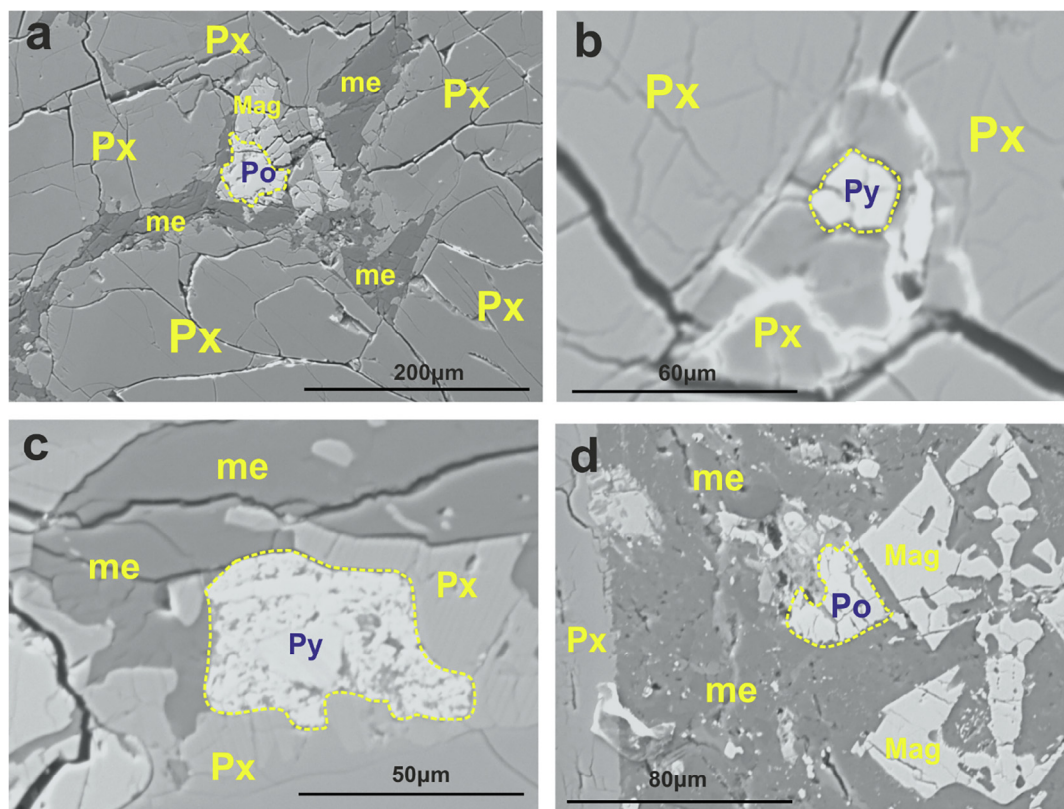


Fig. 2. Backscatter electron (BSE) images of sulphides in Nakhla, Lafayette, and MIL 090032 showing their petrographic relationships with the other minerals. Sulphides that have been selected for sulphur isotopic analysis are rimmed in yellow. A) pyrrhotite (Po) grain in Nakhla; B, C) Pyrite (Py) grains in Lafayette; D) pyrrhotite grain in MIL 090032. Po, pyrrhotite; Py, pyrite; Px, pyroxene (augite); Mag, magnetite; me, mesostasis. (For interpretation of the references to colour in this figure legend, the reader is referred to the web version of this article.)

Greenwood et al. (2000b) for pyrrhotite grains in Nakhla agree well with our values, having a range in  $\Delta^{33}\text{S} = -0.4 \pm 0.5$  to  $-0.07 \pm 0.5\text{‰}$  and a  $\delta^{34}\text{S} = -4.5 \pm 0.4$  to  $1.4 \pm 0.4\text{‰}$ .

Similar to Nakhla, two pyrrhotite grains in Y-000749 gave an average  $\Delta^{33}\text{S} = -0.10 \pm 0.15\text{‰}$  and  $\delta^{34}\text{S} = -1.1 \pm 0.11$ , while only one pyrrhotite was analysed for Y-000593 ( $\Delta^{33}\text{S} = -0.18 \pm 0.07\text{‰}$ ;  $\delta^{34}\text{S} = -1.3 \pm 0.08$ ). Lafayette pyrite analysis (five grains) yielded a range of values in  $\Delta^{33}\text{S} = -0.26$  to  $0.04\text{‰}$  and a  $\delta^{34}\text{S} = -13.2$  to  $-8.53\text{‰}$ , with an average  $\Delta^{33}\text{S} = -0.09 \pm 0.12\text{‰}$ , which approaches the  $\Delta^{33}\text{S} = 0.07\text{‰}$  in Lafayette pyrite analysed by Farquhar et al. (2000). Sulphur isotope data obtained for five grains of MIL 090032 show a  $\Delta^{33}\text{S} = -0.76$  to  $-0.62\text{‰}$  and a  $\delta^{34}\text{S} = 7.60$  to  $15.1\text{‰}$ , with an average  $\Delta^{33}\text{S} = -0.67 \pm 0.10\text{‰}$  and  $\delta^{34}\text{S} = 10.5\text{‰}$ . Previous measurements via chemical extractions from the four paired Miller Range nakhlites gave a range of  $\Delta^{33}\text{S}$  from  $-0.43$  to  $-0.53\text{‰}$ , in particular an earlier study of the MIL 090136 material gave values that are in the range of our own analysis, with an average  $\Delta^{33}\text{S} = -0.4\text{‰}$  and  $\delta^{34}\text{S} = 7.66\text{‰}$  (Franz et al., 2014; Dottin III et al., 2018).

### 3.3. Rhenium-Os isotope systematics and HSE

Lafayette and Nakhla have broadly similar CI-normalized HSE patterns (Fig. 3a), with a general depletion

of Os, Ir, and Ru relative to Pd and Re (Table 2). However, osmium normalised to CI-chondrite/10,000 ( $\text{Os}_\text{N}$ ) is slightly more abundant (1.69) in Lafayette than in Nakhla (0.25). Osmium, Ir, Ru, and Pt are in agreement with earlier HSE-abundance studies of Nakhla (as reviewed by Jones et al., 2003), with the exception of Pd and Re that show higher abundances in our new data (2.24 and 0.117 ppb, respectively). In general, Os, Ir, Ru, and Pt in Nakhla fall in the range between previous HSE analyses of Nakhla by Dale et al. (2012) and Jones et al. (2003). Platinum, Pd, and Re of Nakhla and Lafayette show similarities with measured Pt and Pd in Chassigny (Jones et al., 2003). Nakhla has the highest  $(\text{Re}/\text{Ir})_\text{N} = 148$  and  $(\text{Pt}/\text{Ir})_\text{N} = 96$  among the studied set of samples, while Lafayette has the highest value in  $(\text{Os}/\text{Ir})_\text{N} = 3.44$  for these nakhlites (Fig. 5). The MIL 090032 CI-normalised HSE pattern is slightly different from the patterns of Nakhla and Lafayette, with higher absolute Os, Ir, and Ru, and Pt (4.54 ppb) having the highest CI-chondrite normalised value.

Nakhla and Lafayette display different Re and Os abundances and Re-Os isotope systematics (Table 2; Fig. 3b). Lafayette has a  $^{187}\text{Re}/^{188}\text{Os}$  and  $^{187}\text{Os}/^{188}\text{Os}$  of  $6 \pm 6$  and  $0.1849 \pm 0.0003$  (uncertainties are expressed as  $2\sigma$  internal precision), respectively. Nakhla is characterized by the highest  $^{187}\text{Re}/^{188}\text{Os}$  value of  $49 \pm 49$  and an  $^{187}\text{Os}/^{188}\text{Os}$  of  $0.4542 \pm 0.0018$ . Despite large uncertainties on  $^{187}\text{Re}/^{188}\text{Os}$



Table 1

S-isotopic compositions for pyrrhotite and pyrite in Nakhla, Lafayette, MIL 090032, Y-000749, and Y-000593.

Sample	Phase	$\delta^{34}\text{S}$ (‰)	$\pm 2\sigma$	$\delta^{33}\text{S}$ (‰)	$\pm 2\sigma$	$\Delta^{33}\text{S}$ (‰)	$\pm 2\sigma$
Nakhla	Pyrrhotite	−0.4	0.11	−0.33	0.08	−0.12	0.08
Nakhla	Pyrrhotite	−2.2	0.10	−1.15	0.08	0.02	0.07
Nakhla	Pyrrhotite	−1.0	0.09	−0.55	0.09	−0.03	0.09
Nakhla	Pyrrhotite	−2.5	0.11	−1.36	0.08	−0.06	0.08
Nakhla	Pyrrhotite	−1.7	0.08	−0.97	0.08	−0.08	0.07
Mean		−1.5		−0.87		−0.05	
Variance		0.62		0.14		0.00	
Lafayette	Pyrite	−13.2	0.10	−6.78	0.09	0.03	0.08
Lafayette	Pyrite	−10.1	0.11	−5.51	0.08	−0.26	0.08
Lafayette	Pyrite	−10.7	0.30	−5.65	0.19	−0.12	0.24
Lafayette	Pyrite	−8.5	0.11	−4.56	0.09	−0.16	0.09
Lafayette	Pyrite	−11.1	0.10	−5.72	0.12	0.04	0.11
Mean		−10.7		−5.64		−0.09	
Variance		2.28		0.49		0.01	
MIL090032	Pyrrhotite	7.6	0.08	3.25	0.08	−0.65	0.07
MIL090032	Pyrrhotite	9.7	0.08	4.34	0.08	−0.65	0.06
MIL090032	Pyrrhotite	9.9	0.10	4.33	0.09	−0.76	0.08
MIL090032	Pyrrhotite	15.2	0.11	7.14	0.18	−0.62	0.18
MIL090032	Pyrrhotite	10.2	0.08	4.58	0.08	−0.69	0.07
Mean		10.5		4.73		−0.67	
Variance		6.22		1.66		0.00	
Yamato000749	Pyrrhotite	−1.6	0.08	−0.83	0.13	0.00	0.13
Yamato000749	Pyrrhotite	−0.9	0.11	−0.59	0.13	−0.08	0.13
Yamato000749	Pyrrhotite	−0.9	0.14	−0.71	0.20	−0.23	0.20
Mean		−1.1		−0.71		−0.10	
Variance		0.09		0.00		0.00	
Yamato000593	Pyrrhotite	−0.7	0.07	−0.57	0.07	−0.21	0.05
Yamato000593	Pyrrhotite	−2.0	0.08	−1.19	0.10	−0.16	0.09
Mean		−1.3		−0.88		−0.18	
Variance		0.42		0.09		0.00	

Data on  $\delta^{34}\text{S}$ ,  $\delta^{33}\text{S}$ , and  $\Delta^{33}\text{S}$  values are expressed in permil (‰) and associated  $2\sigma$  standard errors are reported. Uncertainties count statistics. The mean in sulphur isotope abundance for each meteorite is also shown. Sulphur isotope ratios are reported in standard  $\delta$  notation with respect to Canyon Diablo Troilite (CDT), where  $\delta^{34}\text{S} = [(^{34}\text{S}/^{32}\text{S})_{\text{sample}} / (^{34}\text{S}/^{32}\text{S})_{\text{CDT}} - 1] \times 1000$ ,  $\delta^{33}\text{S} = [(^{33}\text{S}/^{32}\text{S})_{\text{sample}} / (^{33}\text{S}/^{32}\text{S})_{\text{CDT}} - 1] \times 1000$ , and  $\Delta^{33}\text{S} = [(^{33}\text{S}/^{32}\text{S})_{\text{sample}} / (^{33}\text{S}/^{32}\text{S})_{\text{CDT}} - (^{34}\text{S}/^{32}\text{S})_{\text{sample}} / (^{34}\text{S}/^{32}\text{S})_{\text{CDT}}] \times 1000$ .

$\text{Re}/^{188}\text{Os}$  and crystallisation ages  $>1$  Gyr, we tried to calculate the initial  $^{187}\text{Os}/^{188}\text{Os}$  composition of the sample with its percent deviation from the chondritic reference (Shirey and Walker, 1998) using the  $\text{YOs}_i$  notation. The assumed crystallization ages of the most recent  $^{39}\text{Ar}$ – $^{40}\text{Ar}$  dating (Cohen et al., 2017) were used for our calculations. The calculated  $\text{YOs}_i$  is strongly negative. Data on initial  $^{187}\text{Os}/^{188}\text{Os}$  and  $\text{YOs}_i$  are reported in Table 2.

#### 4. DISCUSSION

##### 4.1. Potential for terrestrial alteration and weathering

Some of the nakhlites analysed here could have been affected by alteration during their residence on Earth. In samples recovered from hot deserts the formation of terrestrial clay and carbonate (e.g., Crozaz et al., 2003) can modify lithophile isotope systematics (e.g., Symes et al., 2008) and potentially perturb the Re–Os isotope system. Nakhla was seen to fall, and was recovered shortly thereafter. The provenance of Lafayette is less clear, but its fresh fusion crust suggests it was collected soon after it fell (e.g., Graham et al., 1985). However, even weathering events

lasting a few hours have been shown to cause Re and minor Os redistribution in chondrites from fresh falls (Walker et al., 2018). Terrestrial clays or carbonates are not found within either of these nakhlites, hence the Re–Os isotope system and their sulphides (as supported by our petrographic observations) should not be significantly affected by terrestrial alteration. In addition, initial  $^{87}\text{Sr}/^{86}\text{Sr}$  ratios of Nakhla and Lafayette (0.70254 and 0.70260, respectively) also show little variation (Gale et al., 1975; Shih et al., 1998), suggesting minor or no modification of Sr isotope due to clay and carbonate mineralization.

In contrast, the Miller Range and Yamato nakhlites are Antarctic finds, hence have had greater exposure to the terrestrial environment. The light rare earth element, cerium (Ce) can act as an alteration tracer via the conversion of  $\text{Ce}^{3+}$  to  $\text{Ce}^{4+}$  due to oxidation, with pigeonite being the most susceptible mineral (Crozaz et al., 2003). Cerium anomalies can be found in silicates of the Antarctic Yamato nakhlites (Crozaz et al., 2003), and terrestrially derived jarosite sulphate has been reported towards the exterior of Yamato 000749 (Changela and Bridges, 2011). However, Pb isotope systematics within these nakhlites reflect minimal terrestrial contamination (Yamashita et al., 2002),

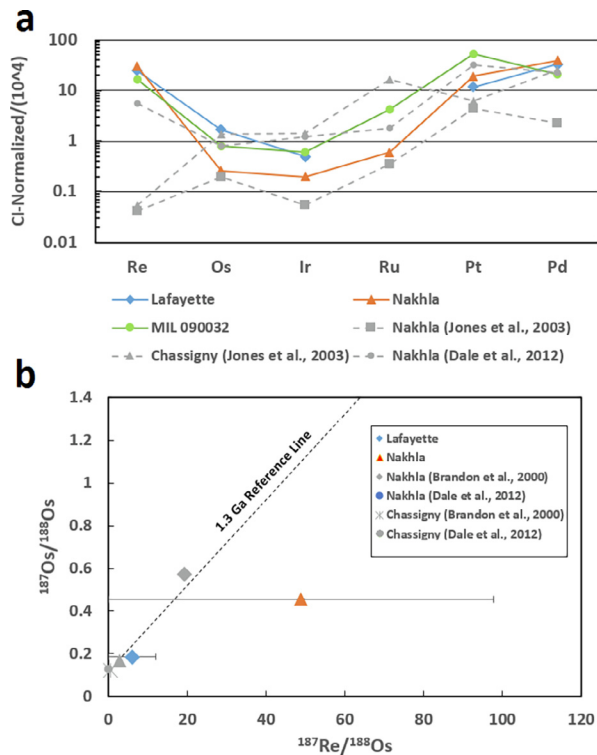


Fig. 3. Highly siderophile element (HSE) abundances and Re-Os isotope systematics in nakhlites. (a) CI chondrite normalized HSE data for Nakhla, Lafayette, and MIL 090032 are shown, along with previously published data in grey (from Jones et al., 2003; Dale et al., 2012); (b)  $^{187}\text{Re}/^{188}\text{Os}$  vs.  $^{187}\text{Os}/^{188}\text{Os}$  data for Nakhla and Lafayette are shown, along with previous literature data (from Brandon et al., 2000; Dale et al., 2012). The 1.3 Ga reference line is shown for comparison and represents single-stage Re-Os isotope evolution from a chondritic  $^{187}\text{Os}/^{188}\text{Os}$  reservoir, assuming a Solar System initial  $^{187}\text{Os}/^{188}\text{Os} = 0.9524$  (Smoliar et al., 1996). Uncertainty =  $2\sigma$ , vertical error bars are less than symbol size.

and the Rb-Sr and Sm-Nd isotope systematics provide little evidence for terrestrial weathering. Olivine and sulphide within the Miller Range nakhlites has suffered aqueous corrosion during residence in Antarctica (Dyar et al., 2005; Hallis and Taylor, 2011; Hallis, 2013; Velbel, 2016). Long exposure to water/snow may have resulted in an addition of anthropogenic radiogenic osmium (Chen et al., 2009). However, terrestrial alteration in the Miller Range nakhlites was considered in previous studies to have no significant impact on the  $\Delta^{33}\text{S}$  and  $\delta^{34}\text{S}$  of its unweathered sulphides, which thereby robustly trace processes on Mars (Dottin III et al., 2018). Hafnium-W isotope values for Nakhla, Lafayette, and MIL 03346 are 0.7–2.25 (Lodders, 1998; Barrat et al., 2006), with a calculated  $\epsilon^{182}\text{W}$  of  $3.13 \pm 0.30$  for Nakhla (Lee and Halliday, 1997) and of  $-2.95 \pm 0.08$  for MIL 03346 (Wadhwa and Borg, 2006), thus demonstrating minor variation and minimal Hf-W isotope disturbance between these nakhlites.

The potential effects of terrestrial alteration on HSE abundances and Re-Os isotopic compositions are addressed in Section 4.3.1.

## 4.2. Origin of sulphur isotopic anomalies in sulphides of nakhlites

The variation of  $\Delta^{33}\text{S}$  and  $\delta^{34}\text{S}$  in the nakhlites, in reference to our dataset, could be due to differences in the chemistry of the atmosphere and surface or alteration by subsurface martian fluids (Farquhar et al., 2000; Franz et al., 2014). To have confidence in which of our nakhlite HSE and Re-Os isotope data are the most representative of the martian magma source(s) for nakhlite meteorites, it is useful to know the extent to which each nakhlite might have been affected by regolith assimilation; where with ‘regolith’ we refer to heterogeneous, unconsolidated, and relatively superficial martian surface deposits.

### 4.2.1. Isotopic fractionation of $\Delta^{33}\text{S}$ in sulphides of nakhlites

Our analyses of Nakhla, Lafayette, MIL 090032, Y-000749, and Y-000593 sulphide grains gave mean  $\Delta^{33}\text{S}$  values of  $-0.05 \pm 0.08\text{‰}$ ,  $-0.09 \pm 0.12\text{‰}$ ,  $-0.67 \pm 0.10\text{‰}$ ,  $-0.10 \pm 0.15\text{‰}$ , and  $-0.18 \pm 0.07\text{‰}$ , respectively (Fig. 4a). Assuming that some of these sulphide grains may be more isotopically fractionated than others, it is important to determine whether the sulphur isotopic signatures are representative of the sample as a whole, and if they are magmatic or non-magmatic in origin.

Appraisal of the petrographic characteristics of our studied samples prior to SIMS analyses showed that we sampled a representative set of pyrite and pyrrhotite grains in terms of textural associations, but that we observed a bias toward grains  $>10\text{ }\mu\text{m}$  in size. Virtually, the magma involved in the generation of the nakhlites can be considered as affected by a degree of crustal assimilation coincident with eruption onto the martian surface (e.g., Franz et al., 2014). The challenge is to disentangle the degree to which the chemistries of the analysed nakhlites were affected by assimilation during the transit of magmas through Mars’ crust and during eruptive processes.

Anomalous sulphur is constrained by its mass-independent fractionation (MIF) signature. Large variations in  $\delta^{34}\text{S}$  can modify the  $\Delta^{33}\text{S}$  of a sulphide by chemical mixing. However, it has been demonstrated that the values of  $\delta^{34}\text{S}$  in martian meteorites do not vary enough to be able to explain the observed variation in  $\Delta^{33}\text{S}$  (Farquhar et al., 2000; Farquhar et al., 2007; Franz et al., 2014). Detection of MIF or non-MIF signatures for sulphur could be constrained by the displacement of non-zero values of  $\Delta^{33}\text{S}$  for each meteorite analysed here, where a magmatic only  $\Delta^{33}\text{S}$  is characterized by near zero values (i.e.,  $\Delta^{33}\text{S} = 0$ ). Lafayette has zero ( $0.03 \pm 0.08\text{‰}$ ) to slightly negative ( $-0.26 \pm 0.08\text{‰}$ )  $\Delta^{33}\text{S}$  in its sulphide grains. This inter-grain variation in Lafayette is the largest heterogeneity in  $\Delta^{33}\text{S}$  of the meteorite dataset that we analysed, implying the presence of both non-MIF (i.e., magmatic) and MIF signatures (assimilation) in Lafayette sulphur. In the case of MIF signatures, these were likely induced by assimilation of regolith-derived sulphur (including regolith affected by brines) during emplacement of Lafayette lava flow on the martian surface. Though relevant for the present-day Mars, data from NASA’s Curiosity rover shows a  $\delta^{34}\text{S}$  with a



Table 2  
Re-Os isotope systematics and HSE abundances (in ppb) for all samples.

	Lafayette	Sample Nakhla	MIL 090032
Mass (g)	0.417	0.405	0.5
Os (blk %)	0.078 (0.70)	0.012 (4.20)	0.036 (1.3)
Ir (blk %)	0.022 (0.10)	0.009 (0.26)	0.025 (24)
Ru (blk %)	—	0.04 (9.89)	0.27 (3.8)
Pt (blk %)	1.01 (0.40)	1.66 (0.25)	4.54 (1.1)
Pd (blk %)	1.89 (1)	2.24 (0.87)	1.18 (17.5)
Re (blk %)	0.098 (0.49)	0.117 (0.42)	0.065 (8.4)
Rh (blk %)	—	—	0.21 (2.9)
Au (blk %)	—	—	0.081 (24)
$^{187}\text{Re}/^{188}\text{Os}$ ( $\pm 2\sigma$ )	6 (6)	49 (49)	—
$^{187}\text{Os}/^{188}\text{Os}$ ( $\pm 2\sigma$ )	0.1849 (0.0003)	0.4542 (0.0018)	—
$\gamma\text{Os}_i$ ( $\pm 2\sigma$ )	−64 (34.3)	−636 (5)	—
Re/Os	1	10	2
Pt/Os	12.9	138.3	126.1
Os/Ir	3.54	1.33	1.44
(Pt/Pd)N	0.35	0.48	2.51
(Pd/Os)N	19.6	131.3	26
$\varepsilon^{143}\text{Nd}$ ( $\pm 2\sigma$ )	16.3 (0.4)	16	—
Age (Ma) ( $\pm 2\sigma$ )	1383 (7)	1330 (15)	1392 (10)
Lab	Durham	Durham	Berlin

$\gamma\text{Os}_i$  is given by  $\gamma\text{Os}_i = 100 \times [(^{187}\text{Os}/^{188}\text{Os}_{\text{sample}(t)}) / (^{187}\text{Os}/^{188}\text{Os}_{\text{chondrite}(t)}) - 1]$ . HSE ratios normalized to Orgueil chondrite are denoted by (N). Initial  $^{143}\text{Nd}$  are from Nakamura et al. (1982) and Shih et al. (1998). Ages are from Cohen et al. (2017).

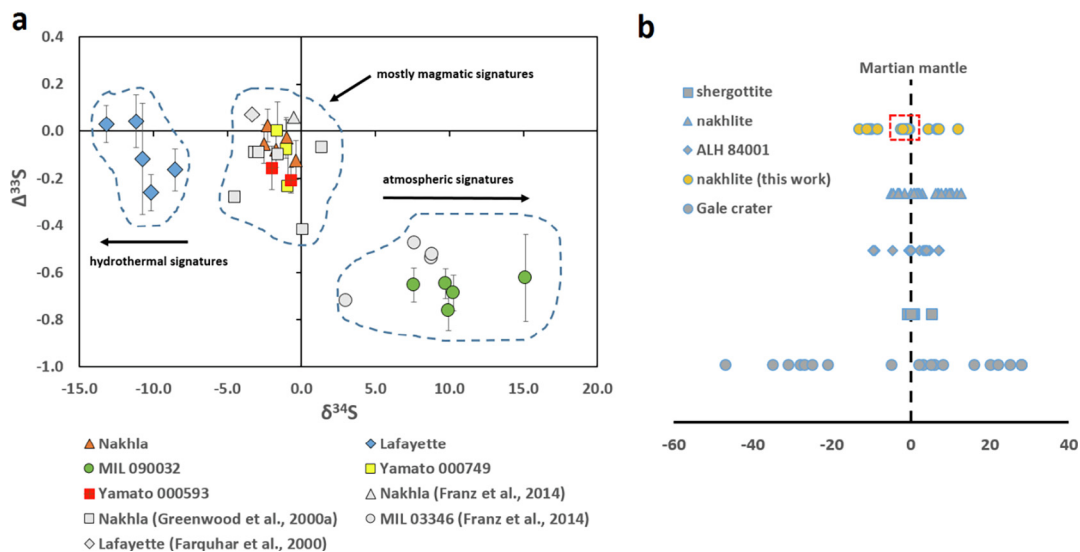


Fig. 4. Sulphur isotope ratios for the nakhrites, compared with previous data from Martian meteorites and Mars rover missions data. (a)  $\delta^{34}\text{S}$  vs.  $\Delta^{33}\text{S}$  isotope ratios for the nakhrites analysed in this work, compared with the same nakhrites analysed by previous authors. Labels serve to emphasise which processes are inferred to have affected the sulphur isotopic composition of each data cluster.  $2\sigma$  uncertainties are shown, with X-axis uncertainties smaller than the symbols; (b) Comparison of  $\delta^{34}\text{S}$  value between the present study (yellow symbols) and literature data from martian meteorites (Farquhar et al., 2000; Greenwood et al., 2000a; Franz et al., 2014; Franz et al., 2017) and the Curiosity rover (Franz et al., 2017). The  $\delta^{34}\text{S}$  value of the martian mantle (from Franz et al., 2014) is shown by the dashed line. The red box identifies the nakhrites that have a  $\delta^{34}\text{S}$  very close to the martian mantle  $\delta^{34}\text{S}$  value and so have been least affected by regolith assimilation (Nakhla, Y-000749, and Y-000593). Some of the data used in the graphs are from previous studies (Farquhar et al., 2000; Greenwood et al., 2000a; Franz et al., 2014; Franz et al., 2017). (For interpretation of the references to colour in this figure legend, the reader is referred to the web version of this article.)

range far in excess of that observed among nakhrites (−47 to 28‰; Franz et al., 2017), it is reasonable to conclude that these observations imply that the assimilation of even a small percentage of Mars' regolith at the time of nakhrite

formation could significantly shift the sulphur isotopic composition of these nakhrites (by several ‰).

For Nakhla we obtained a  $\Delta^{33}\text{S}$  equal to zero ( $-0.05 \pm 0.08\text{‰}$ ,  $n = 5$ ), suggesting a magmatic origin (non-MIF

signature) for all sulphur in Nakhla. This value is in accordance with a previously reported mean  $\Delta^{33}\text{S}$  of  $0.06\text{‰}$  for Nakhla sulphides (Franz et al., 2014). However, Nakhla is internally variable and some of the studied sulphides show more negative  $\Delta^{33}\text{S}$ , with  $\Delta^{33}\text{S}$  as low as  $-0.33\text{‰}$  and  $-0.4\text{‰}$  (Greenwood et al., 2000a,b; Franz et al., 2014). We report similar near zero values of  $\Delta^{33}\text{S}$  from the three sulphide grains in Y-000749 (average  $\Delta^{33}\text{S} = -0.10 \pm 0.15\text{‰}$ ; with one sulphide having a magmatic  $\Delta^{33}\text{S} = 0.00 \pm 0.13\text{‰}$ ) and from the sulphide grain in Y-000593 ( $\Delta^{33}\text{S} = -0.18 \pm 0.07\text{‰}$ ). However, we were not able to analyse sulphide grains smaller than  $10\text{ }\mu\text{m}$  in these nakhlites and  $\Delta^{33}\text{S}$  values may be somewhat internally variable. Based on the analysed sulphide grains, we suggest a non-primordial mantle sulphur signal but still a dominantly magmatic origin for the sulphur isotopic systematics of Nakhla, Y-000749, and Y-000593, without large extents of regolith assimilation during their magmatic emplacement. Miller Range 090032 represents the meteorite with the most marked MIF signatures in sulphide grains, with a negative mean  $\Delta^{33}\text{S}$  of  $-0.67 \pm 0.10\text{‰}$ , with wide variability between grains (Fig. 4). Large variability in  $\Delta^{33}\text{S}$  in sulphides of the Miller Range paired nakhlites is also in agreement with Franz et al. (2014) and Dottin III et al. (2018). These values suggest that sulphides in MIL 090032 are affected by MIF signatures, probably caused by secondary processes that occurred on Mars (Mikouchi et al., 2003), as suggested by Franz et al. (2014) for the paired stone MIL 03346. Secondary processing possibilities are explored below.

#### 4.2.2. Isotopic fractionation of $\delta^{34}\text{S}$ in sulphides of nakhlites

The absence of crustal recycling on Mars may have been effective in leaving heterogeneous sulphur signatures on the surface. Sulphur isotope ratios can be fractionated by three main processes: hydrothermal (e.g., Ohmoto and Goldhaber, 1997), photochemical (e.g., Zmolek et al., 1999; Farquhar et al., 2001), and biological (e.g., Parnell et al., 2010). In addition to these processes, we discuss also possible magmatic processes that can fractionate  $\delta^{34}\text{S}$ . Large isotopic fractionations of  $\delta^{34}\text{S}$  have been investigated recently by the NASA's Curiosity rover from a 13 km long transect in Gale Crater (Franz et al., 2017). The measured  $\delta^{34}\text{S}$  ranged from  $-47 \pm 14\text{‰}$  to  $28 \pm 7\text{‰}$  (Fig. 4b); whether the negative values occurred in sulphides and the positive values occurred in sulphates or sulphites (mudstone and sandstone) is yet to be resolved. The reason Curiosity reported a greater range in  $\delta^{34}\text{S}$  than that observed in martian meteorites is probably due to the accumulation of fine crustal materials in Gale crater following long periods of fluvial and/or aeolian transport.

Nakhlite sulphur isotopic signatures have been interpreted as reflecting both equilibrium fractionation in a warmed martian groundwater environment (low  $\delta^{34}\text{S}$ ) or atmospheric photochemical processes (high  $\delta^{34}\text{S}$ ) (Franz et al., 2017). In particular, the  $\delta^{34}\text{S}$  enrichment is reported to derive from atmospheric processing of  $\text{SO}_2$  and  $\text{H}_2\text{S}$  via martian volcanic activity (processes capable of producing positive  $\delta^{34}\text{S}$  signatures) with subsequent incorporation of these products into the martian surface/subsurface

(Franz et al., 2017, see Fig. 2). This was also deduced experimentally (Franz et al., 2013) and from oxidation of  $\text{SO}_2$  in volcanic ashes (Savarino, 2003).

Fractionation of  $\delta^{34}\text{S}$  differs for all the five nakhlites analysed here (Fig. 4b). However, it is important to notice that the  $\delta^{34}\text{S}$  variation could not be a full signature of the contaminant. It is possible that S loss processes can fractionate  $\delta^{34}\text{S}$ , and such processes would not be expected to significantly shift the  $\Delta^{33}\text{S}$ . Thus, the  $\delta^{34}\text{S}$  of the samples with the most anomalous  $\Delta^{33}\text{S}$  might reflect a different combination of processes, related to addition of sulphur, that would exert the first order control on  $\Delta^{33}\text{S}$ , and then loss of sulphur that would exert a first order control on  $\delta^{34}\text{S}$  due to kinetic stable isotopic fractionation. Sulphides in Nakhla, Y-000749, and Y-000593 have the most convincing magmatic signatures, being characterized by a near zero mean  $\delta^{34}\text{S}$  (mean  $-1.59 \pm 0.10\text{‰}$ ,  $-1.18 \pm 0.11\text{‰}$ , and  $-1.36 \pm 0.08\text{‰}$ , respectively), supported also from their magmatic  $\Delta^{33}\text{S}$  values described above. Conversely, MIL 090032 has an enriched  $\delta^{34}\text{S}$  (mean  $+10.54 \pm 0.09\text{‰}$ ), that is the largest intra-meteorite variation in sulphur isotopic fractionation and the largest positive  $\delta^{34}\text{S}$  value obtained in a martian material ( $+15.2 \pm 0.1\text{‰}$ ). These values suggest enrichment of  $\delta^{34}\text{S}$  due to martian atmospheric processes characterised by oxidation of  $\text{H}_2\text{SO}_4$  or photolysis of sulphur compounds (gases) introduced by volcanic eruptions and outgassing (Savarino, 2003; Franz et al., 2017). This finding is similar to reported measurements of  $\delta^{34}\text{S}$  fractionation close to the vents of terrestrial volcanoes ( $+7.7 \pm 0.8\text{‰}$ ; Mather et al., 2006).

Lafayette has the greatest  $\delta^{34}\text{S}$  depletion yet described for a martian meteorite (average of  $-10.7 \pm 0.2\text{‰}$ ), with values of  $\delta^{34}\text{S}$  reaching  $-13.2 \pm 0.1\text{‰}$  – and lower than the Allan Hills (ALH) 84001,  $\delta^{34}\text{S}$  values ( $\sim -9\text{‰}$ ) previously reported for pyrite grains (Greenwood et al., 2000a). These values are suggestive of late-stage equilibrium fractionation with martian groundwater, consistent with the Lafayette  $\Delta^{33}\text{S}$  results. Previous analysis of Lafayette reported values of  $\delta^{34}\text{S}$  of  $-3.2 \pm 2.1\text{‰}$  (Greenwood et al., 2000b; Farquhar et al., 2000). The greater depletion in our  $\delta^{34}\text{S}$  values may reflect heterogeneous assimilation of sulphur from the martian regolith. Alternatively (or in addition), Lafayette sulphides have 'spongy' textures (Fig. 2c), which could be the product of alteration by shock melting with subsequent volatilisation effects (e.g., Gattacceca et al., 2013). Both Greenwood et al. (2000b) and Farquhar et al. (2000) proposed mixing of fluids with heavy ( $\delta^{34}\text{S} > 0$ ) and light sulphur ( $\delta^{34}\text{S} < 0$ ) as a hydrothermal process that can produce negative  $\delta^{34}\text{S}$ . Some of the nakhlite lava flows may have been in contact with, or in close proximity, to a heavy sulphur source, while, in general, all may have been affected by mixing with fluids characterized by contrasting  $\delta^{34}\text{S}$  values.

At temperatures  $< 1200\text{ }^\circ\text{C}$  the magmatic degassing of  $\text{SO}_2$  can modify the sulphur isotope ratios of magmas (Sakai et al., 1982), depending on the  $f\text{O}_2$  (Carroll and Webster, 1994). Two cases are possible: (1) if  $f\text{O}_2 \gg$  quartz-fayalite-magnetite (QFM) buffer, sulphate is the dominant sulphur phase in the magma. The consequent equilibrium isotopic fractionation factor will be positive

( $\Delta\text{SO}_4^2 - \text{SO}_2 > 0$ ; Sakai et al., 1982), hence the residual melt is enriched in  $\delta^{34}\text{S}$  due to  $\text{SO}_2$  degassing, producing sulphides enriched in  $\delta^{34}\text{S}$ . (2) If  $f\text{O}_2 = \text{QFM}$  or  $f\text{O}_2 < \text{QFM}$  sulphide is the dominant sulphur phase in the magma, with consequent negative equilibrium isotopic fractionation factor ( $\Delta\text{S}_2 - \text{SO}_2 < 0$ ; Sakai et al., 1982). In this way, the melt may become depleted in  $\delta^{34}\text{S}$ . This mechanism leads to crystallization of sulphides that are depleted in  $\delta^{34}\text{S}$ . Magmatic degassing could have been the cause of the positive  $\delta^{34}\text{S}$  signature in MIL 090032, by shifting the  $\text{SO}_4$  in the silicate melt structure sulphates can be reduced to yield more positive  $\delta^{34}\text{S}$  values (see Labidi et al., 2015; Mandeville et al., 2009; Dottin III et al., 2018), that was subsequently reduced to form the sulphides.

#### 4.2.3. Assimilation versus acquisition of martian regolith during lava emplacement

The  $\Delta^{33}\text{S}$  and  $\delta^{34}\text{S}$  values presented here (Fig. 4), along with the fact that nakhlite sulphides are associated with the mesostasis (hence are some of the last phases to crystallise) (Chevrier et al., 2011; Fig. 2), indicate assimilation of an S-rich martian regolith occurred within at least some of the nakhlite lava flows (Lafayette and MIL 090032). The range in  $\Delta^{33}\text{S}$  among the nakhlites may be broadly related to the total sulphur content of each lava flow, where nakhlites with larger  $\Delta^{33}\text{S}$  anomalies were in proximity of a “sulphur source”, contrary to nakhlites with smaller  $\Delta^{33}\text{S}$  anomalies (Dottin III et al., 2018). This sulphur source could be represented by the S-rich martian regolith (Foley et al., 2003). Sulphides also occur in several different sizes and modal abundances in all nakhlite meteorites. In the meteorite samples studied sulphide grain sizes range from 10  $\mu\text{m}$  to 250  $\mu\text{m}$  (Fig. 2). The recently recovered nakhlite Caleta el Cobre 022 has unusually abundant and coarse grained pyrrhotite (up to 200  $\mu\text{m}$ ) (Gattacceca et al., 2018). These inter-meteorite differences in sulphide grain sizes are therefore further evidence to support the suggestion that sulphur-rich material was acquired at different points of lava extrusion on the martian surface.

Nakhla and the two Yamato nakhlites contain dominantly magmatic sulphur isotope signatures (near zero  $\Delta^{33}\text{S}$  and  $\delta^{34}\text{S}$ ), indicating a lack of regolith incorporation. A  $^{17}\text{O}$  excess of sulphate in Nakhla reportedly suggests it spent a significant period of time in contact with the Martian atmosphere (Farquhar et al., 2000). The simplest way of reconciling this atmospheric exposure with minimal regolith uptake is to place Nakhla at the top of a lava flow. Alternatively, it could have been present inside the carapace of a lava tube, where the main flow is in contact with the surface and easily acquires sulphide/sulphate material from the Martian regolith while the carapace of the lava tube is never in contact with the regolith but can be in contact with the atmosphere. This hypothesis could also explain the regolith uptake of MIL 090032, if it was part of the main lava tube. These two nakhlites have the same age (within uncertainty; Cohen et al., 2017), but they have different  $\delta^{34}\text{S}$  (Nakhla =  $-1.59 \pm 0.10\text{‰}$ , MIL 090032 =  $+10.54 \pm 0.09\text{‰}$ ). This lava emplacement scenario is supported by the quench-textured mesostasis of MIL 090032 and the other paired MIL nakhlites, indicating surface exposure

(Hallis and Taylor, 2011), possibly as a break-out event at the front or side of the lava flow (Hammer, 2009). Further, skeletal mineral phases, glass, and thin hedenbergite pyroxene rims in the MIL nakhlites has been taken as evidence of the fastest cooling rate among all the nakhlites (6  $^\circ\text{C}/\text{h}$ ) (Hammer and Rutherford, 2005; Day et al., 2006). Alternatively, if the MIL nakhlites and Nakhla are not from the same lava flow, mineralogical evidence suggests that after quenching the MIL nakhlite lava flow may have been blanketed with another flow that slowed down the cooling rate (Domenech et al., 2013) – this flow may have been that containing Nakhla.

#### 4.2.4. $\Delta^{33}\text{S}$ of the nakhlite mantle source

Nakhla and the two Yamato meteorites have  $\delta^{34}\text{S}$  close to zero, and the smallest fractionation of  $\Delta^{33}\text{S}$ . This signature is interpreted to have a magmatic origin, hence these meteorites represent the least isotopically disturbed of the nakhlites analysed here (from a sulphur isotope perspective), and by inference the most appropriate to constrain a possible  $\Delta^{33}\text{S}$  for the nakhlite mantle source region. The average  $\Delta^{33}\text{S}$  value obtained for Nakhla, Yamato 000749, and Yamato 000,593 sulphide grains is  $-0.1 \pm 0.09\text{‰}$ . This is slightly more negative than the shergottite mantle source value ( $\Delta^{33}\text{S}$  of 0.009 $\text{‰}$ ) calculated by Franz et al. (2014), possibly due to the fact that different mantle reservoirs were involved in the genesis of the shergottites and the nakhlites (e.g., Harper et al., 1995; Lee and Halliday, 1997; Wadhwa, 2001; Jones et al., 2003; Foley et al., 2005).

It is unlikely that a  $\Delta^{33}\text{S}$  of a mantle reservoir shifted by 0.1 $\text{‰}$  from an initial value of zero. Instead, we attribute this  $\Delta^{33}\text{S}$  value to contamination by mass-independent sulphur that would have originated in the martian atmosphere (Farquhar et al., 2000). It is conceivable that such atmospheric sulphur ( $\text{SO}_2$ ,  $\text{H}_2\text{S}$ ), after its deposition as oxidized sulphur on the martian surface, could have affected the source of the nakhlite magmas by mobilization beneath the martian crust due to geochemical cycling, therefore suggesting the presence of a shallow magma chamber for the generation of the nakhlites.

### 4.3. Constraining the magmatic and chemical-physical processes in controlling Re-Os isotope systematics and HSE

Several different chemical-physical processes may have influenced the HSE-abundance Re-Os isotope systematics of the nakhlites. These processes can be distinguished essentially as: low-temperature disturbance(s), post-crystallization impact disturbance, and HSE partitioning under magmatic conditions. To discriminate which of these processes may have affected each of our samples, and to what degree, we discuss each sequentially and begin by appraising those processes that could modify the HSE and Re-Os isotope chemistry of a magmatic sample after its crystallisation.

#### 4.3.1. Low-temperature and post-crystallization impact disturbance

Late-stage open-system effects on nakhlite HSE due to alteration on Mars' or Earth's surface have the potential



to disturb nakhlite Re-Os isotope systematics and to mobilise and/or add HSE present in potentially susceptible phases. For example, the possibility of low-temperature alteration in deserts could result in the addition of Re (Peucker-Ehrenbrink and Jahn, 2001) (Fig. 3). However, there is limited variation of inter-element HSE ratios and we conclude that nakhlite HSE-abundance has not been significantly affected by low-temperature alteration on Earth or Mars after their magmatic crystallisation.

Impact disturbance as considered here refers to the process(es) through which materials of chondritic composition are transferred to martian magmatic materials due to impacts/shock events after their crystallisation. Such processes are capable of enriching the sample toward chondrite-relative HSE abundances following magmatic crystallisation (e.g. as was observed by Riches et al., 2012). All studied nakhlites are characterised by highly fractionated HSE patterns relative to CI-chondrite (e.g., Pd/Os = 19.6–131.3), have relatively low total osmium abundances (<0.08 ppb), and suprachondritic  $^{187}\text{Os}/^{188}\text{Os}$  (0.18–0.45  $\pm$  0.0010). These nakhlite HSE characteristics do not tend toward a potential chondritic contaminant and thereby preclude significant late-stage modification of the studied samples by chondritic materials on the martian surface or during their impact liberation.

#### 4.3.2. Magmatic processes

All three nakhlites analysed in this work display similar HSE patterns. It is unlikely that these similarities in HSE patterns are the product of alteration on Earth or Mars, instead these primarily reflect magmatic fractionation during formation of the nakhlite parent magma(s) and lava crystallisation. These nakhlite HSE characteristics indicate that the incorporation of small amounts of martian regolith (as testified by S-isotope systematics) resulted in a generally negligible modification to the nakhlite HSE inventory, suggesting a low HSE abundance of the martian regolith. Had significant contributions of regolith modified the overall HSE abundances of the studied nakhlites, we would anticipate variable HSE systematics among the nakhlites and a degree of correlation with sulphide S-isotope compositions. Such nakhlite HSE variability and a clear relationship to corresponding sulphide S-isotope systematics is lacking. However, Os-isotope compositions of nakhlites are variable and are decoupled from the overall nakhlite HSE-abundance systematics. The intra-sample variability in Re concentration and Os-isotopic composition testified by two Nakhla fractions (0.117 ppb, this work; 0.052, Brandon et al., 2000) supports perturbation of the Re-Os isotope systematics in these martian magmas, but with little consequent effect to the abundances of Os, Ru, Ir, Pt, Pd,  $\pm$  Au. Such a process requires interaction with a martian regolith of variable Re content and low Os abundance, but with highly radiogenic  $^{187}\text{Os}/^{188}\text{Os}$  (>0.7 at total HSE abundances much less than 2 ppb and with 0.005 ppb Os in the ancient martian regolith) such that a small proportion of assimilated material has perturbed the Os-isotopic signature of the nakhlite lava flows. Fractionation of HSE during partial melting of the mantle and during possible late-sulphide saturation in evolved magmas will change

HSE inventories in different ways (Jones et al., 2003; Sun et al., 2003; Fonseca et al., 2007; Mallmann and O'Neill, 2007). In the following sub-paragraphs we explore these possible processes.

**4.3.2.1. Magmatic fractionation of HSE from the nakhlite and shergottite mantle source.** Regression approaches using MgO content have been used to infer Mars mantle composition and give similar abundances of Re, Os, Ir, and Ru for the mantle of Earth and Mars (e.g., Warren et al., 1999; Tait and Day, 2018). In addition, martian meteorites are characterised by Re abundances that are high, somewhat close to the terrestrial basalts, and define a broad anticorrelation of HSE abundances with the degree of magmatic evolution (e.g., Jones et al., 2003). Several prior studies have appraised martian magmatic process through the HSE abundances of martian meteorites (e.g. Warren et al., 1999; Jones et al., 2003; Riches et al., 2011; Brandon et al., 2012; Dale et al., 2012; Filiberto et al., 2012; Tait et al., 2015; Tait and Day, 2018). In general, what the HSE datasets of these previous studies show are CI-normalised HSE patterns that vary from absolutely flat to increasingly fractionated (elevated Pd/Os) with decreasing total HSE abundance.

Nakhla, Lafayette, and MIL 090032 all show broadly similar HSE patterns (Fig. 3a). Though previous data showed that Nakhla and Chassigny are similar in their HSE patterns (Jones et al., 2003), here isotope dilution approaches show that Nakhla has more Pd and Re relative to Chassigny and that Lafayette and MIL 090032 are very similar to this pattern, rather than the HSE pattern of Chassigny. These substantial differences in the HSE fractionation evident among different classes of martian meteorite and thus their magmas, extended also to shergottite groups. Primitive shergottites (Mg/Mg + Fe > 0.7) have high Os/Pt, Ir/Pd and Ru/Pt (Brandon et al., 2012; Tait and Day, 2018). A broadly similar pattern was observed for the high MgO shergottites (Mg/Mg + Fe = 0.5–0.7), but with higher Re/Pt and Re/Pd than the primitive shergottites. Nakhlites analysed here diverge from the patterns of the primitive and high MgO shergottites in terms of relative abundances, but they approach the HSE patterns of the intermediate/low MgO shergottites having high Re/Ir, Pt/Ir, and Pd/Ru (Fig. 5). These differences could reflect different initial magmatic conditions between the nakhlite and shergottite parental melt(s), as for example, melting temperature,  $f\text{O}_2$ , and parental melt composition (including sulphur concentration and its relation to the point of sulphide saturation). We address the possible late-stage sulphide saturation as well as potential involvement of residual alloys during the production of magmas parental to nakhlite lavas below.

**4.3.2.2. HSE fractionation due to late-stage sulphide saturation and residual alloys formation.** Sulphides, silicate phases, and spinel can control the geochemical behaviour of the HSE during partial melting (Fonseca et al., 2007; Mallmann and O'Neill, 2007), with Os inclined to be partitioned into sulphide melts (Brenan, 2008). The solubility of Os and Ir has been constrained experimentally in sulphide

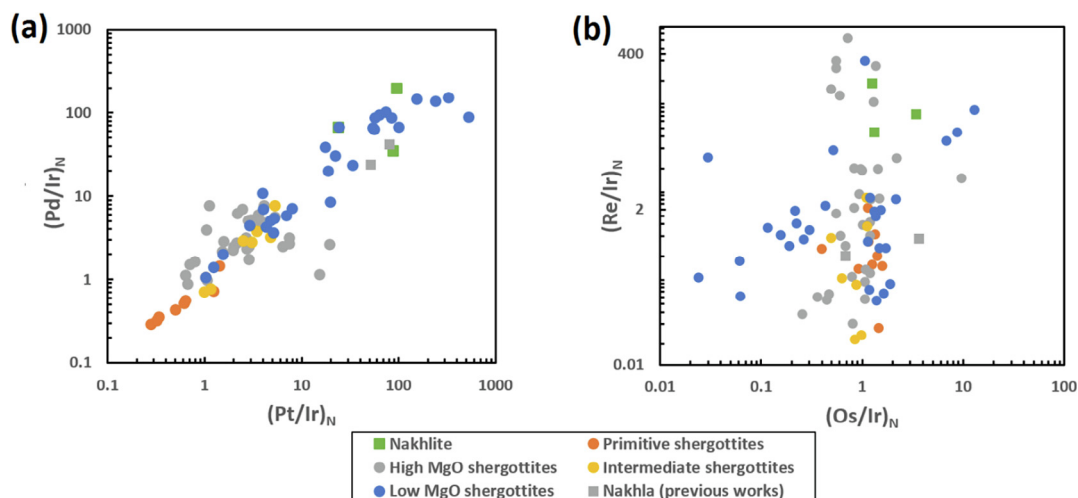


Fig. 5. CI chondrite normalized HSE abundance comparison between nakhrites, primitive shergottites ( $Mg/Mg + Fe > 0.7$ ), high MgO shergottites ( $Mg/Mg + Fe = 0.5–0.7$ ), shergottites with intermediate MgO ( $Mg/Mg + Fe = 0.4–0.5$ ), and low MgO shergottites ( $Mg/Mg + Fe < 0.4$ ). (a)  $(Pt/Ir)_N$  vs.  $(Pd/Ir)_N$ ; (b)  $(Os/Ir)_N$  vs.  $(Re/Ir)_N$ . The nakhrites plot closest to the low MgO shergottites in (a), and within the scatter of these shergottites in (b). Highly siderophile element data for shergottites are from Jones et al. (2003), Riches et al. (2011), Brandon et al. (2012), Dale et al. (2012), and Tait and Day (2018).

melts, over a range of  $fO_2$  ( $-1.5 < QFM < +1.5$ ) and  $fS_2$  (Iron-Wüstite (IW)  $\sim -1$ ) at  $T = 1300^\circ C$  (Fonseca et al., 2011). It is important to take into account that these experimental approaches can generally only replicate batch melting, and that a fractional melting scenario ( $\pm$ aggregation of those fractional melts) may be applicable to both ancient and recent martian magmatic systems. Nevertheless, experimental approaches provide a useful framework through which we can infer key aspects of nakhrite petrogenesis. The outcome of these experiments has shown that Os and Ir have low solubilities in silicate melts and that high  $fO_2$  conditions can inhibit the solubility of Os and Ir in sulphide melts (Fonseca et al., 2011). Oxygen fugacity for nakhrites is higher than shergottites. For Nakhla,  $fO_2$  is equal to the quartz-fayalite-magnetite (QFM) oxygen buffer (at an equilibration temperature of  $810^\circ C$ ) while for Lafayette the  $fO_2$  is equal to  $QFM + 0.1$  (at an equilibration temperature of  $780^\circ C$ ; Szymanski et al., 2010). For MIL 03346 (paired with MIL 090032) the proportion of  $Fe^{3+}$  in augite was found to be in agreement with high-temperature equilibration near the QFM buffer (Dyar et al., 2005). Conversely, estimated  $fO_2$  for the shergottites are low and varies from  $-1$  to  $-4$  QFM (e.g., Herd, 2003). These differences in  $fO_2$  would limit the solubility of Os and Ir in nakhrite sulphide melts, due to their higher  $fO_2$  than shergottites.

Residual alloys crystallised from parental melts and the formation of platinum group minerals throughout a magmatic column are able to control fractionation of Os, Ir, Ru, Rh, Pt, and Pd during magma genesis (Mungall and Brennan, 2014). In particular, Mungall and Brennan (2014) reported how, at low pressure, partial melting of Earth's mantle retains HSE in chondritic relative abundances (if correct as the starting proportions of these elements) until complete sulphide saturation, then evolving to very high Pt/Pd and low Pd/Ir – due to Pt and Ir alloy formation in the restite phase. Ruthenium, Os, and Ir are thought to

be initially present in parts per million abundances in mantle sulphide melts, then, a decrease in  $fS_2$  during partial melting leads to the exsolution of Ru-Os-Ir alloys from a refractory residue in the mantle (Fonseca et al., 2012). In particular, a sulphide melt appears to be required for Os-rich alloy formation since Os is likely the element that triggers the exsolution of the Ru-Os-Ir alloys (Fonseca et al., 2012).

As described above, the higher  $fO_2$  in Nakhla, Lafayette, and MIL 090032 likely prevented the solubility of Os and Ir in possible late-stage sulphide melts, inducing formation of Pt- and Ir-alloys in the restite phase. Accordingly to Fonseca et al. (2011), the higher solubility of Os and Ir at high  $fO_2$  would imply the existence of a melt saturated in sulphides (sulphide melt) for the generation of the nakhrite parent magmas. In contrast to nakhrite magmas, for which present data sets and constraints are relatively limited, it is well established that the parent magmas of the relatively well-studied shergottites were sulphide-undersaturated in their mantle sources (Wang and Becker, 2017). In particular, Pd/Pt in shergottites tend to reflect chondritic abundances, but this is not the case for Os-Ir-Ru, as indicated by suprachondritic Pd/Ir or Pt/Ir (Wang and Becker, 2017). The reason of this difference could be attributed to the formation of residual alloys of Os-Ir-Ru in the martian mantle (similar to the Earth's mantle; e.g., Fonseca et al., 2012 and references therein).

#### 4.4. Implications for nakhrite mantle source and early Mars differentiation

Mantle heterogeneities have been proposed for Mars based on the trace element and  $^{182}Hf$ - $^{182}W$ ,  $^{146}Sm$ - $^{142}Nd$ ,  $^{87}Rb$ - $^{87}Sr$ , and  $^{187}Re$ - $^{187}Os$  isotope systematics of magmatic products represented by martian meteorites (e.g., Harper et al., 1995; Lee and Halliday, 1997, 1995; Brandon et al.,

2000, 2012; Wadhwa, 2001; Herd, 2003; Jones et al., 2003; Foley et al., 2005; Debaille et al., 2008, 2009; Herd et al., 2017; Lapen et al., 2017; Tait and Day, 2018; Day et al., 2018). In general, at least four mantle reservoirs have been previously argued to exist on Mars: two for the shergottites, one for the nakhlites/chassignites, and one for NWA 8159. These different mantle domains can be tapped by magmas and these magmas can mix producing different compositions as noticeable from the different groups of martian meteorites.

Magma mixing phenomena have been argued to be responsible of the generation of the depleted and enriched shergottites (Borg et al., 1997; Wadhwa, 2001; Herd, 2003; Borg and Draper, 2003; Shearer et al., 2008). However, the clear isotopic gaps that are present for their lithophile elements (Ferdous et al., 2017) are difficult to reconcile with magma mixing, since this process would not result in large isotopic gaps. This is especially noticeable for the nakhlites since they do not present clear signs of disequilibrium textures in their mineral assemblages. Instead, we propose a single magma composition for the generation of the nakhlites (as also suggested by their trace element compositions; Udry and Day, 2018), whether after the Nakhla eruption assimilation with an unknown enriched component affected the nakhlite source during 61 Myr, producing subsequently the Lafayette parent melt at  $1321 \pm 9$  Ma (ages accordingly to Cohen et al., 2017).

Assimilation of crustal materials with markedly elevated  $^{187}\text{Re}/^{188}\text{Os}$  could be a cause of the higher  $^{187}\text{Re}/^{188}\text{Os}$  of Nakhla in respect to Lafayette. This enriched component

possibly included ancient (primordial?) crustal materials, with consequent highly radiogenic Os isotopic compositions for which a very small fraction would significantly shift a magmatic Os isotopic signature but with potentially negligible effects on HSE abundances. On the other hand, this characteristic could also reflect phenomena of mantle metasomatism as recently argued for Mars magmatism (Day et al., 2018), or even inheritance from an interior reservoir that experienced variable earlier magmatic fractionation resulting in reservoirs with long-term high  $^{187}\text{Re}/^{188}\text{Os}$  and/or complementary low  $^{187}\text{Re}/^{188}\text{Os}$ .

Mixing within mantle sources or enriched cumulates may have happened during early differentiation of Mars. By following this logic, the enriched crustal component of our hypothesis likely can be represented by a component generated during the last stages of a martian magma ocean (MMO). This possibility has been investigated for Nakhla and Lafayette by looking at their  $^{187}\text{Os}/^{188}\text{Os}$  versus Nd and Sr isotope distributions. The  $\text{YOs}$  versus  $\epsilon^{143}\text{Nd}$  constrain a possible end-member for the nakhlite source mixing. The calculated  $\text{YOs}$  and  $\epsilon^{143}\text{Nd}$  values of the primitive martian crust and the evolved Martian crust at 180 Ma from Brandon et al. (2000) and Norman (1999) were used (Fig. 6). The distribution of the nakhlites in respect to the primitive and evolved martian crust is inconsistent with their magma sources being affected by assimilation of modern martian crust. The  $\text{YOs}$  vs.  $\epsilon^{143}\text{Nd}$  appear instead decoupled suggesting preferential/selective mixing of the nakhlite reservoir with an unknown enriched component that must have occurred early during Mars differenti-

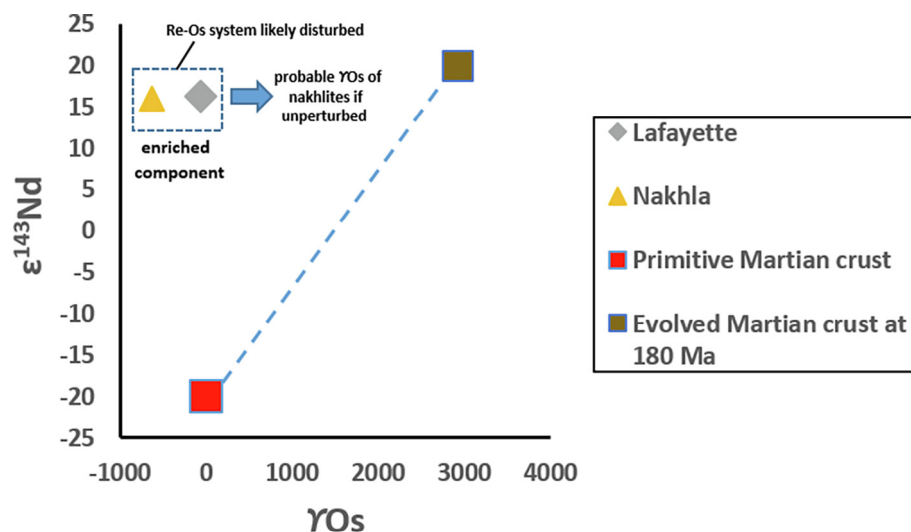


Fig. 6. Initial  $\text{YOs}$  vs.  $\epsilon^{143}\text{Nd}$  for nakhlites used to identify a possible end-member for the nakhlite source mixing. The primitive martian crust and the evolved martian crust at 180 Ma are plotted with values taken from Brandon et al. (2000) and Norman (1999). The plotted samples follow a direction that diverge from the martian crust evolution (here represented by the dashed line), thus implying that the mixing end-member is likely represented by a different enriched component (dashed box) rather than the evolved martian crust. Alternatively, decoupling of the data could suggest that the  $\text{YOs}$  is a sensitive tracer of strictly different process to that which  $\epsilon^{143}\text{Nd}$  provides evidence – potentially recording involvement of early martian crust whereas  $\epsilon^{143}\text{Nd}$  may be more effective in probing the nature of nakhlite mantle reservoirs. Error bars are less than symbol size. As the calculated  $\text{YOs}$  in Lafayette and Nakhla is negative and below the Solar System initial of Smoliar et al. (1996) disturbance of the Re-Os isotope system in these samples has taken place (linked to crustal contamination). For these reasons, the strongly negative calculated  $\text{YOs}$  should be considered as an extreme minimum at  $\sim 1.4$  Ga. Unperturbed samples, not impacted by crustal assimilation, would likely have been derived from internal reservoirs characterized by higher  $\text{YOs}$  at that time (blue arrow). (For interpretation of the references to colour in this figure legend, the reader is referred to the web version of this article.)



ation, possibly represented by assimilated ancient MMO cumulates. However, drawing conclusions from the initial  $\text{YOs}$  for Nakhla and Lafayette are currently thwarted by large uncertainties for these relatively ancient magmas with low Os abundances. Similarly, the correlation between  $\varepsilon^{143}\text{Nd}$  and  $\text{YOs}$  in shergottites suggested that the endmember sources were generated by mixing between residual melts and cumulates during the crystallization stages of a MMO (Debaille et al., 2008; Brandon et al., 2012).

Mixing within MMO cumulates and evolved liquids may explain our observed Re-Os isotope systematics as seen in Nakhla and Lafayette, as well as previously reported Rb and Sr isotope systematics. In fact, sulphides crystallisation from the last stage of MMO's melts could result in locally fractionated  $^{187}\text{Re}/^{188}\text{Os}$  within the martian mantle thereby presenting the possibility to trace different mantle reservoirs and to discern this from assimilation of primordial crust characterized by long-term elevated  $^{187}\text{Re}/^{188}\text{Os}$ . In addition, the first MMO cumulates that crystallize would be extremely depleted in REE, Rb and Sr, with the last more evolved liquids characterised by a  $\varepsilon^{142}\text{Nd}$  of +0.64 (Debaille et al., 2009).

Magma ocean overturn could explain the early formation and isolation of these different local heterogeneities in the martian mantle (Debaille et al., 2009; Bouvier et al., 2018). This process likely happens as a result of instabilities due to the density stratification that occurs during the crystallisation of magma oceans on terrestrial planets (Elkins-Tanton et al., 2003).

## 5. CONCLUSIONS

Sulphur isotopic compositions were determined for sulphides in five nakhlites to ascertain the degree to which they have been affected by assimilation of the martian regolith. Nakhla, Yamato 000749, and Yamato 000593 are the meteorites that have most faithfully retained a magmatic signature, and which are therefore the most reliable for using osmium isotopes and HSEs to reveal the nature of nakhlite petrogenesis. For the first time, Re-Os isotope systematics and HSE abundances have been investigated for two different nakhlites, to constrain the degree to which they have been affected by crustal assimilation and the ability of martian meteorite HSE to testify to Mars' interior composition. The following results have been obtained:

- (1) The Lafayette and MIL 090032 lava flows acquired S-rich martian regolith material that carry information about martian atmospheric and hydrological processes. Results show that UV-photochemistry and hydrothermal processes are the main cause of  $\Delta^{33}\text{S}$  and  $\delta^{34}\text{S}$  fractionation. This result may have implications for the nature of the martian atmosphere and hydrothermal activity prior to nakhlite eruption.
- (2) Nakhla, Yamato 000593, and Yamato 000749 retained a magmatic signature in their sulphides, and were unaffected by assimilation of martian regolith. Using these meteorites we estimate the  $\Delta^{33}\text{S}$  of the nakhlite source to be  $-0.1\%$ .

- (3) Nakhlite HSE patterns are in agreement with the presence of a sulphide melt involved in nakhlite petrogenesis. Ruthenium-Os-Ir alloys likely formed in this sulphide-saturated melt and controlled the abundances of Ru, Os, Ir in the final lava products.
- (4) Our Re-Os isotope data for nakhlites hint at perturbation and potential decoupling of nakhlite  $^{187}\text{Os}/^{188}\text{Os}$  isotope systematics from other isotopic systems as a result of small degrees of assimilation of an S-rich regolith with low total HSE contents but highly radiogenic  $^{187}\text{Os}/^{188}\text{Os}$  ( $>0.7$  at total HSE abundances much less than 2 ppb and with 0.005 ppb Os in the ancient martian regolith).
- (5) Nakhlites formed from a primary magma that we consider to have been generated from a well-mixed martian mantle that subsequently (at some point after the Nakhla emplacement) assimilated an enriched component during ascent toward the surface, and where this enriched mantle material was potentially represented by a late-stage crystallization cumulate from a martian magma ocean.

## ACKNOWLEDGEMENT

We are grateful to NASA – ANSMET for providing the Miller Range samples, to the Natural History Museum of London for allocation of the Nakhla and Lafayette samples, and to JAXA for providing the Yamato 000749 and Yamato 000593 samples. We thank P. Chung for its help during SEM-EDS analysis. AJVR was supported on an Independent Fellowship thanks to funding from the European Union's Horizon 2020 Research and Innovation Programme under the Marie Skłodowska-Curie grant agreement No. 653066. Analytical work at FUB was funded by CRC TRR 170-B1. This is TRR 170 publication no. 51. We also acknowledge funding from STFC grants ST/N000846/1 and ST/H002960/1. We thank the Editor James M.D. Day for the useful comments and suggestions that improved the quality of the manuscript. We thank James Farquhar and the anonymous reviewers for their review of this manuscript. AJVR thanks Larry Taylor, to whom this Special Issue is dedicated, for enthusiastically introducing her to planetary science studies for which she has developed an addiction.

## APPENDIX A. SUPPLEMENTARY MATERIAL

Supplementary data to this article can be found online at <https://doi.org/10.1016/j.gca.2019.05.025>.

## REFERENCES

- Barrat J. A., Benoit M. and Cotton J. (2006) Bulk chemistry of the Nakhlite Miller Range 03346 (MIL 03346). *Lunar Planet. Sci. XXXVII*. Lunar Planet. Inst., Houston, #1569(abstr.).
- Berkley J. L., Kiel K. and Prinz M. (1980) Comparative petrology and origin of Governador Valadares and other nakhlites. In *Proc. Lunar Planet. Sci. Conf. 11th*, pp. 1089–1102.
- Birck J. L. and Allegre C. J. (1994) Contrasting Re/Os magmatic fractionation in planetary basalts. *Earth Planet. Sci. Lett.* **124**, 139–148.

- Birck J. L., Roy-Barman M. and Capman F. (1997) Re–Os isotopic measurements at the femtomole level in natural samples. *Geostand. Newslett.* **20**, 19–27.
- Boctor N. Z., Meyer H. O. A. and Kullerud G. (1976) Lafayette meteorite: petrology and opaque mineralogy. *Earth and Planetary Science Letters* **32**, 69–76.
- Borg L. E. and Draper D. S. (2003) A petrogenetic model for the origin and compositional variation of the Martian basaltic meteorites. *Meteoritics Planet. Sci.* **38**, 1713–1731.
- Borg L. E., Nyquist L. E., Taylor L. A., Wiesmann H. and Shih C. Y. (1997) Constraints on Martian differentiation processes from Rb–Sr and Sm–Nd isotopic analyses of the basaltic shergottite QUE94201. *Geochimica et Cosmochimica Acta* **61**, 4915–4931.
- Bottke W. F., Walker R. J., Day J. M. D., Nesvorný D. and Elkins-Tanton L. (2010) Stochastic late accretion to Earth, the Moon, and Mars. *Science* **330**(6010), 1527–1530.
- Bouvier L. C., Costa M. M., Connelly J. N., Jensen N. K., Wielandt D., Storey M., Nemchin A. A., Whitehouse M. J., Snape J. F., Bellucci J. J., Moynier F., Agranier A., Gueguen B., Schönbachler M. and Bizzarro M. (2018) Evidence for extremely rapid magma ocean crystallization and crust formation on Mars. *Nature* **558**, 586–589.
- Bunch T. E. and Reid A. M. (1975) The Nakhilites, I. Petrography and mineral chemistry. *Meteoritics* **10**, 303–315.
- Brandon A. D., Puchtel I. S., Walker R. J., Day J. M. D., Irving A. J. and Taylor L. A. (2012) Evolution of the martian mantle inferred from the 187Re–187Os isotope and highly siderophile element abundance systematics of shergottite meteorites. *Geochimica et Cosmochimica Acta* **76**, 206–235.
- Brandon A. D., Walker R. J., Morgan J. W. and Goles G. G. (2000) Re–Os isotopic evidence for early differentiation of the Martian mantle. *Geochimica et Cosmochimica Acta* **64**(23), 4083–4095.
- Brenan J. M. (2008) Re–Os fractionation by sulfide melt silicate melt partitioning: a new spin. *Chem. Geol.* **248**, 140–165.
- Bridges J. C. and Grady M. M. (2000) Evaporite mineral assemblages in the nakhilite (martian) meteorites. *Earth Planet. Sci. Lett.* **176**, 267–279.
- Carroll M. R. and Webster J. D. (1994) Solubilities of sulfur, noble gases, nitrogen, chlorine, and fluorine in magmas. In *Volatiles in Magmas*. Mineral. Soc. Amer., Washington, DC, pp. 231–280.
- Changela H. G. and Bridges J. C. (2011) Alteration assemblages in the nakhilites: Variation with depth on Mars. *Meteorit. Planet. Sci.* **45**, 1847–1867.
- Chen C., Sedwick P. N. and Sharma M. (2009) Anthropogenic osmium in rain and snow reveals global-scale atmospheric contamination. *Proc. National Acad. Sci.* **106**(19), 7724–7728.
- Chevrier V., Lorand J. P. and Sautter V. (2011) Sulfide petrology of four nakhilites: Northwest Africa 817, Northwest Africa 998, Nakhla, and Governador Valadares. *Meteorit. Planet. Sci.* **46**(6), 769–784.
- Chu Z. Y., Yan Y., Chen Z., Guo J. H., Yang Y. H., Li C. F. and Zhang Y. B. (2015) A comprehensive method for precise determination of Re, Os, Ir, Ru, Pt, Pd concentrations and Os isotopic compositions in geological samples. *Geostand. Geoanal. Res.* **39**, 151–169.
- Clark B. C., Baird A. K., Rose H. J., Toulmin, III, P., Keil K., Castro A. J., Kelliher W. C., Rowe C. D. and Evans P. H. (1976) Inorganic analyses of Martian surface samples at the Viking landing sites. *Science* **194**, 1283–1288.
- Cohen A. S. and Waters F. G. (1996) Separation of osmium from geological materials by solvent extraction for analysis by thermal ionisation mass spectrometry. *Anal. Chim. Acta* **332**, 269–275.
- Cohen B. E., Mark D. F., Cassata W. S., Lee M. R., Tomkinson T. and Smith C. L. (2017) Taking the pulse of Mars via dating of a plume-fed volcano. *Nature Commun.* **8**(640), 1–9.
- Corrigan C. M., Velbel M. A. and Vicenzi E. P. (2015) Modal abundances of pyroxene, olivine, and mesostasis in nakhilites: heterogeneity, variation, and implications for nakhilite emplacement. *Meteorit. Planet. Sci.* **50**(9), 1497–1511.
- Crozaz G., Floss C. and Wadhwa M. (2003) Chemical alteration and REE mobilization in meteorites from hot and cold deserts. *Geochimica et Cosmochimica Acta* **67**, 4727–4741.
- Dale C. W., Burton K. W., Greenwood R. C., Gannoun A., Wade J., Wood B. and Pearson D. G. (2012) Late accretion on the earliest planetesimals revealed by the highly siderophile elements. *Science* **336**, 72–75.
- Day J. M. D., Taylor L. A., Floss C., McSween H. Y., Liu Y. and Hill E. (2005) Petrogenesis of Martian Nakhilite MIL 03346. *Meteorit. and Planet. Sci.* **40** abstract, #5288.
- Day J. M. D., Tait K. T., Udry A., Moynier F., Liu Y. and Neal C. R. (2018) Martian magmatism from plume metasomatized mantle. *Nature Commun.* **9**, 4799.
- Day J. M. D., Brandon A. D. and Walker R. J. (2016) Highly siderophile elements in Earth, Mars, the Moon, and Asteroids. *Rev. Mineral. Geochem.* **81**, 161–238.
- Day J. M. D., Taylor L. A., Floss C. and McSween H. Y. (2006) Petrology and chemistry of MIL 03346 and its significance in understanding the petrogenesis of nakhilites on Mars. *Meteorit. Planet. Sci.* **41**(4), 581–606.
- Debaille V., Yin Q. Z., Brandon A. D. and Jacobsen B. (2008) Martian mantle mineralogy investigated by the 176Lu–176Hf and 147Sm–143Nd systematics of shergottites. *Earth Planet. Sci. Lett.* **269**, 186–199.
- Debaille V., Brandon A. D., O'Neill C., Yin Q. Z. and Jacobsen B. (2009) Early martian mantle overturn inferred from isotopic composition of nakhilite meteorites. *Nature Geosci.* **2**, 548–552.
- Domenechetti M. C., Fioretti A. M., Camara F., McCammon C. and Alvaro M. (2013) Thermal history of nakhilites: A comparison between MIL 03346 and its terrestrial analogue Theo's flow. *Geochimica et Cosmochimica Acta* **121**, 571–581.
- Dottin, III, J. W., Labidi J., Farquhar J., Piccoli P., Liu M. C. and McKeegan K. D. (2018) Evidence for oxidation at the base of the nakhilite pile by reduction of sulfate salts at the time of lava emplacement. *Geochimica et Cosmochimica Acta* **239**, 186–197.
- Dyar M. D., Treiman A. H., Pieters C. M., Hiroi T., Lane M. D. and O'Connor V. (2005) MIL 03346, the most oxidized Martian meteorite: A first look at spectroscopy, petrography, and mineral chemistry. *J. Geophys. Res.* **110**, E09005.
- Elkins-Tanton L. T., Parmentier E. M. and Hess P. C. (2003) Magma ocean fractional crystallization and cumulate overturn in terrestrial planets: Implications for Mars. *Meteorit. Planet. Sci.* **38**(12), 1753–1771.
- Farquhar J., Kim S. T. and Masterson A. (2007) Implications from sulfur isotopes of the Nakhla meteorite for the origin of sulfate on Mars. *Earth Planet. Sci. Lett.* **264**, 1–8.
- Farquhar J., Savarino J., Jackson T. L. and Thiemens M. H. (2000) Evidence of atmospheric sulphur in the martian regolith from sulphur isotopes in meteorites. *Nature* **404**, 50–52.
- Farquhar J., Savarino J., Sabine A. and Thiemens M. H. (2001) Observation of wavelength-sensitive mass-independent sulfur isotope effects during SO<sub>2</sub> photolysis: Implications for the early atmosphere. *J. Geophys. Res.* **106**, 32829–32839.
- Ferdous J., Brandon A. D., Peslier A. H. and Pirotte Z. (2017) Evaluating crustal contributions to enriched shergottites from the petrology, trace elements, and Rb–Sr and Sm–Nd isotope systematics of Northwest Africa 856. *Geochimica et Cosmochimica Acta* **211**, 280–306.

- Filiberto J., Chin E., Day J. M. D., Franchi I. A., Gross J., Greenwood R. C., Penniston-Dorland S., Schwenzer S. and Treiman A. (2012) Geochemistry of intermediate olivine-phyric shergottite northwest Africa 6234, with similarities to basaltic shergottite northwest Africa 480 and olivine-phyric shergottite northwest Africa 2990. *Meteorit. Planet. Sci.* **47**, 1256–1273.
- Fischer-Gödde M., Becker H. and Wombacher F. (2010) Rhodium, gold and other highly siderophile element abundances in chondritic meteorites. *Geochimica et Cosmochimica Acta* **74**, 356–379.
- Fischer-Gödde M., Becker H. and Wombacher F. (2011) Rhodium, gold and other highly siderophile elements in orogenic peridotites and peridotite xenoliths. *Chem. Geol.* **280**, 365–383.
- Foley C. N., Economou T. and Clayton R. N. (2003) Final chemical results from the Mars Pathfinder Alpha Proton X-ray Spectrometer. *J. Geophys. Res.* **108**, 8096.
- Foley C. N., Wadhwa M., Borg L. E., Janney P. E., Hines R. and Grove T. L. (2005) The early differentiation history of Mars from 182W–142Nd isotope systematics in the SNC meteorites. *Geochimica et Cosmochimica Acta* **69**, 4557–4571.
- Fonseca R. O. C., Mallmann G., O'Neill H. S. C., Campbell I. H. and Laurenz V. (2011) Solubility of Os and Ir in sulphide melt: implications for Re/Os fractionation in the upper mantle. *Earth Planet. Sci. Lett.* **311**, 339–350.
- Fonseca R. O. C., Laurenz V., Mallmann G., Luguet A., Hoehne N. and Jochum K. P. (2012) New constraints on the genesis and long-term stability of Os-rich alloys in the Earth's mantle. *Geochimica et Cosmochimica Acta* **87**, 227–242.
- Fonseca R. O. C., Mallmann G., O'Neill H. S. C. and Campbell I. H. (2007) How chalcophile is rhenium? An experimental study of the solubility of Re in sulfide mattes. *Earth Planet. Sci. Lett.* **260**, 537–548.
- Franz H. B., Danielache S. O., Farquhar J. and Wing B. A. (2013) Mass-independent fractionation of sulfur isotopes during broadband SO<sub>2</sub> photolysis: comparison between 16O- and 18O-rich SO<sub>2</sub>. *Chem. Geol.* **362**, 56–65.
- Franz H. B., Sang-Tae K., Farquhar J., Day J. M. D., Economos R. C., McKeegan K. D., Schmitt A. K., Irving A. J., Hoek J. and Dottin J. (2014) Isotopic links between atmospheric chemistry and the deep sulphur cycle on Mars. *Nature* **508**, 364–368.
- Franz H. B., McAdam A. C., Ming D. W., Freissinet C., Mahaffy P. R., Eldridge D. L., Fischer W. W., Grotzinger J. P., House C. H., Hurowitz J. A., McLennan S. M., Schwenzer S. P., Vaniman D. T., Archer P. D., Atreya S. K., Conrad P. G., Dottin, III, J. W., Eigenbrode J. L., Farley K. A., Glavin D. P., Johnson S. S., Knudson C. A., Morris R. V., Navarro-González R., Pavlov A. A., Plummer R., Rampe E. B., Stern J. C., Steele A., Summons R. E. and Sutter B. (2017) Large sulfur isotope fractionations in Martian sediments at Gale crater. *Nature Geosci.* **10**, 658–662.
- Gattacceca J., Devouard B., Debaille V., Rochette P., Lorand J. P., Bonal L., Beck P., Sautter V., Meier M. M. M., Gounelle M., Marrocchi Y., Maden C. and Busemann H. (2018) Nakhilite Caleta el Cobre 022: initial description and comparison with other nakhlites. *81st Annual Meeting of The Meteoritical Society 2018*, #6227(abstr.).
- Gale N. H., Arden J. W. and Hutchison R. (1975) The chronology of the Nakhla achondritic meteorite. *Earth Planet. Sci. Lett.* **26**, 195–206.
- Gattacceca J., Hewins R. H., Lorand J. P., Rochette P., Lagroix F., Cournede C., Uehara M., Pont S., Sautter V., Scorzelli R. B., Hombourger C., Munayco P., Zanda B., Channaoui H. and Ferrière L. (2013) Opaque minerals, magnetic properties, and paleomagnetism of the Tissint Martian meteorite. *Meteorit. Planet. Sci.* **48**, 1919–1936.
- Graham A. L., Bevan A. W. R. and Hutchison R. (1985) Catalogue of Meteorites, fourth ed. British Museum (Natural History). Univ. Arizona Press, Tucson.
- Greenwood J. P., Mojzsis S. J. and Coath C. D. (2000a) Sulfur isotopic compositions of individual sulfides in Martian meteorites ALH 84001 and Nakhla: implications for crust–regolith exchange on Mars. *Earth Planet. Sci. Lett.* **184**, 23–35.
- Greenwood J. P., Riciputi L. R., McSween H. Y. and Taylor L. A. (2000b) Modified sulfur isotopic compositions of sulfides in the nakhlites and Chassigny. *Geochimica et Cosmochimica Acta* **64** (6), 1121–1131.
- Hallis L. J. and Taylor G. J. (2011) Comparisons of the four Miller Range nakhlites, MIL 03346, 090030, 090032 and 090136: Textural and compositional observations of primary and secondary mineral assemblages. *Meteorit. Planet. Sci.* **46**(12), 1787–1803.
- Hallis L. J. (2013) Alteration assemblages in the Miller Range and Elephant Moraine regions of Antarctica: comparisons between terrestrial igneous rocks and Martian meteorites. *Meteorit. Planet. Sci.* **48**(2), 165–179.
- Hammer J. E. and Rutherford M. J. (2005) Experimental crystallization of Fe-rich basalt: application to cooling rate and oxygen fugacity of nakhlite MIL 03346. *Lunar Planet. Sci. XXXVI*. Lunar Planet. Inst., Houston, #1999(abstr.).
- Hammer J. E. (2009) Application of a textural geospeedometer to the late-stage magmatic history of MIL 03346. *Meteorit. Planet. Sci.* **44**, 141–154.
- Harper C. L., Nyquist L. E., Bansal B., Weismann H. and Shih C.-Y. (1995) Rapid accretion and early differentiation of Mars indicated by 142Nd/144Nd in SNC meteorites. *Science* **267**, 213–217.
- Herd C. D. K. (2003) The oxygen fugacity of olivine-phyric Martian basalts and the components within the mantle and crust of Mars. *Meteorit. Planet. Sci.* **38**, 1793–1805.
- Herd C. D. K., Walton E. L., Agee C. B., Muttik N., Ziegler K., Shearer C. K., Bell A. S., Santos A. R., Burger P. V., Simon J. I., Tappa M. J., McCubbin F. M., Gattacceca J., Lagroix F., Sanborn M. E., Yin Q.-Z., Cassata W. S., Borg L. E., Lindvall R. E., Kruijer T. S., Brennecka G. A., Kleine T., Nishiizumi K. and Caffee M. W. (2017) The Northwest Africa 8159 martian meteorite: Expanding the martian sample suite to the early Amazonian. *Geochimica et Cosmochimica Acta* **218**, 1–26.
- Jones J. H., Neal C. R. and Ely J. C. (2003) Signatures of the highly siderophile elements in the SNC meteorites and Mars: a review and petrologic synthesis. *Chem. Geol.* **196**, 21–41.
- King P. L. and McLennan S. M. (2010) Sulfur on Mars. *Elements* **6**, 107–112.
- Labidi J., Cartigny P. and Jackson M. G. (2015) Multiple sulphur isotope composition of oxidized Samoan melts and the implications of a sulfur isotope “mantle array” in chemical geodynamics. *Earth Planet. Sci. Lett.* **417**, 28–39.
- Lapen T. J., Richter M., Andreassen R., Irving A. J., Satkoski A. M., Beard B. L., Nishiizumi K., Jull A. J. T. and Caffee M. W. (2017) Two billion years of magmatism recorded from a single Mars meteorite ejection site. *Sci. Adv.* **3**(2), e1600922.
- Lee D. C. and Halliday A. N. (1995) Hafnium-tungsten chronometry and the timing of terrestrial core formation. *Nature* **378**, 771–774.
- Lee D. C. and Halliday A. N. (1997) Core formation on Mars and differentiated asteroids. *Nature* **388**, 854–857.
- Lentz R. C. F., Taylor G. J. and Treiman A. H. (1999) Formation of a Martian pyroxenite: A comparative study of the Nakhilite meteorites and Theo's flow. *Meteorit. and Planet. Sci.* **34**, 919–932.



- Lodders K. (1998) A survey of Shergottite, Nakhilite and Chassigny meteorites whole-rock compositions. *Meteorit. Planet. Sci.* **33**, A183–A190.
- Mallmann G. and O'Neill H. S. C. (2007) The effect of oxygen fugacity on the partitioning of rhenium between crystals and silicate melt during mantle melting. *Geochimica et Cosmochimica Acta* **71**(11), 2837–2857.
- Mandeville C. W., Webster J. D., Tappen C., Taylor B. E., Timbal A., Sasaki A., Hauri E. and Bacon C. R. (2009) Stable isotope and petrologic evidence for open-system degassing during the climactic and pre-climactic eruptions of Mt. Mazama, Crater Lake, Oregon. *Geochimica et Cosmochimica Acta* **73**, 2978–3012.
- Mather T. A., McCabe J. R., Rai V. K., Thiemens M. H., Pyle D. M., Heaton T. H. E., Sloane H. J. and Fern G. R. (2006) Oxygen and sulfur isotopic composition of volcanic sulfate aerosol at the point of emission. *J. Geophys. Res.* **111**, D18205.
- Morgan J. W. (1986) Ultramafic xenoliths: clues to Earth's late accretionary history. *J. Geophys. Res.* **91**, 12375–12387.
- McCubbin F. M., Elardo S. M., Shearer, Jr. C. K., Smirnov A., Hauri E. H. and Draper D. S. (2013) A petrogenetic model for the comagmatic origin of chassignites and nakhilites: Inferences from chlorine-rich minerals, petrology, and geochemistry. *Meteorit. Planet. Sci.* **48**(5), 819–853.
- McDonough W. F. and Sun S. (1995) The composition of the Earth. *Chem. Geol.* **120**, 223–254.
- McSween H. Y. and Huss G. R. (2010) *Cosmochemistry*. Cambridge University Press, Cambridge.
- Mikouchi T., Koizumi E., Monkawa A., Ueda Y. and Miyamoto M. (2003) Mineralogy and petrology of Yamato 000593: Comparison with other martian nakhilite meteorites. *Ant. Met. Res.* **16**, 34–57.
- Mungall J. E. and Brenan J. M. (2014) Partitioning of platinum-group elements and Au between sulfide liquid and basalt and the origins of mantle-crust fractionation of the chalcophile elements. *Geochimica et Cosmochimica Acta* **125**, 265–289.
- Nakamura N., Unruh D. M., Tatsumoto M. and Hutchison R. (1982) Origin and evolution of the Nakhla meteorite inferred from the Sm–Nd and U–Pb systematics and REE, Ba, Sr, Rb and K abundances. *Geochimica et Cosmochimica Acta* **46**, 1555–1573.
- Norman M. D. (1999) The composition and thickness of the crust of Mars estimated from rare earth elements and neodymium-isotopic compositions of Martian meteorites. *Met. Planet. Sci.* **34**, 439–449.
- Ohmoto H. and Goldhaber M. B. (1997) Sulfur and carbon isotopes. In *Barnes, Geochemistry of Hydrothermal Ore Deposits*, third ed. Wiley, pp. 517–611.
- Parnell J., Boyce A., Thackrey S., Muirhead D., Lindgren P., Mason C., Taylor C., Still J., Bowden S., Osinski G. R. and Lee P. (2010) Sulfur isotope signatures for rapid colonization of an impact crater by thermophilic microbes. *Geology* **38**(3), 271–274.
- Pearson D. G. and Woodland S. J. (2000) Solvent extraction/anion exchange separation and determination of PGEs (Os, Ir, Pt, Pd, Ru) and Re–Os isotopes in geological samples by isotope dilution ICP-MS. *Chem. Geol.* **165**(1–2), 87–107.
- Peucker-Ehrenbrink B. and Jahn B. M. (2001) Rhenium–osmium isotope systematics and platinum group element concentrations: loess and the upper continental crust. *Geochem. Geophys. Geosyst.* **2**, 2001GC000172.
- Puchtel I. S., Walker R. J., Brandon A. D. and Irving A. J. (2008) Highly siderophile element abundances in SNC meteorites: an update. *Lunar Planet. Sci. XXXVIII*. Lunar Planet. Inst., Houston, #1650(abstr.).
- Riches A. J. V., Liu Y., Day J. M. D., Puchtel I. S., Rumble D., McSween H. Y., Walker R. J. and Taylor L. A. (2011) Petrology and geochemistry of Yamato 984028: A cumulate ilherzolitic shergottite with affinities to Y 000027, Y 000047, and Y 000097. *Polar Sci.* **4**, 497–514.
- Riches A. J. V., Day J. M. D., Walker R. J., Simonetti A., Liu Y., Neal C. R. and Taylor L. A. (2012) Rhenium–osmium isotope and highly-siderophile-element abundance systematics of angrite meteorites. *Earth Planet. Sci. Lett.* **353–354**, 208–218.
- Righter K., Walker R. J. and Warren P. H. (2000) Significance of highly siderophile elements and osmium isotopes in the lunar and terrestrial mantles. In *Origin of the Earth and Moon* (eds. R. M. Canup and K. Righter). University of Arizona press, Tucson.
- Sakai H., Casadevall T. J. and Moore J. G. (1982) Chemistry and isotope ratios of sulfur in basalts and volcanic gases at Kilauea volcano, Hawaii. *Geochimica et Cosmochimica Acta* **46**, 729–738.
- Savarino J. (2003) UV induced mass-independent sulfur isotope fractionation in stratospheric volcanic sulfate. *Geophys. Res. Lett.* **30**, 2131.
- Shearer C. K., Burger P. V., Papike J. J., Borg L. E., Irving A. J. and Herd C. D. K. (2008) Petrogenetic linkages among Martian basalts: Implications based on trace element chemistry of olivine. *Meteorit. Planet. Sci.* **43**, 1241–1258.
- Stopar J. D., Lawrence S. J., Lentz R. C. F. and Taylor G. J. (2005) Preliminary analysis of Nakhilite MIL03346, with a focus on secondary alteration. *Lunar Planet. Sci.* **36 abstract**, #1547.
- Shih C. Y., Nyquist L. E., Reese Y., Wiesmann H. and Lockheed M. (1998) The chronology of the nakhilite, lafayette: Rb–Sr and Sm–Nd isotopic ages. *Lunar Planet. Sci. XXVIII*. Lunar Planet. Inst., Houston, #1145(abstr.).
- Shirey S. B. and Walker R. J. (1998) The Re–Os isotope system in cosmochemistry and high-temperature geochemistry. *Annu. Rev. Earth Planet. Sci.* **26**, 423–500.
- Smoliar M. I., Walker R. J. and Morgan J. W. (1996) Re–Os ages of Group IIA, IIIA, IVA, and IVB. *Meteorit. Sci.* **271**(5252), 1099–1102.
- Sun W., Bennett V. C., Eggins S. M., Kamenetsky V. S. and Arculus R. J. (2003) Enhanced mantle-to-crust rhenium transfer in undegassed arc magmas. *Nature* **422**, 294–297.
- Symes S., Borg L., Shearer C. and Irving A. (2008) The age of the martian meteorite Northwest Africa 1195 and the differentiation history of the shergottites. *Geochimica et Cosmochimica Acta* **72**, 1696–1710.
- Szymanski A., Brenker F. E., Palme H. and El Goresy A. (2010) High oxidation state during formation of Martian nakhilites. *Meteorit. Planet. Sci.* **45**, 32–42.
- Tait K. T. and Day J. M. D. (2018) Chondritic late accretion to Mars and the nature of shergottite reservoirs. *Earth Planet. Sci. Lett.* **494**, 99–108.
- Tait K. T., Day J. M. D. and Liu Y. (2015) Update on highly-siderophile element abundances and Re–Os isotopic systematics of martian meteorites. *Lunar Planet. Sci. XXXVI*. Lunar Planet. Inst., Houston, #2138(abstr.).
- Treiman A. H., Barrett R. A. and Gooding J. L. (1993) Preterrestrial aqueous alteration of the Lafayette (SNC) meteorite. *Meteoritics* **28**, 86–97.
- Treiman A. H. (1986) The parental magma of the Nakhla achondrite: Ultrabasic volcanism on the shergottite parent body. *Geochimica et Cosmochimica Acta* **50**(6), 1061–1070.
- Treiman A. H. (1990) Complex petrogenesis of the Nakhla (SNC) meteorite: Evidence from petrography and mineral chemistry. *Proc. Lunar Planet. Sci. Conf.* **20**, 273–280.
- Treiman A. H. (2005) The nakhilite meteorites: Augite-rich igneous rocks from Mars. *Chemie der Erde* **65**, 203–270.

- Udry A., McSween H. Y., Lecumberry-Sanchez P. and Bodnar R. J. (2012) Paired nakhlites MIL 090030, 090032, 090136, and 03346: Insights into the Miller Range parent meteorite. *Meteorit. Planet. Sci.* **47**(10), 1575–1589.
- Udry A. and Day J. M. D. (2018) 1.34 billion-year-old magmatism on Mars evaluated from the co-genetic nakhlite and chassignite meteorites. *Geochimica et Cosmochimica Acta* **238**, 292–315.
- Usui T., Alexander C. M. O. D., Wang J., Simon J. I. and Jones J. H. (2012) Origin of water and mantle–crust interactions on Mars inferred from hydrogen isotopes and volatile element abundances of olivine-hosted melt inclusions of primitive shergottites. *Earth Planet. Sci. Lett.* **357–358**, 119–129.
- Velbel M. A. (2016) Aqueous corrosion of olivine in the Mars meteorite Miller Range (MIL) 03346 during Antarctic weathering: Implications for water on Mars. *Geochimica et Cosmochimica Acta* **180**, 126–145.
- Wadhwa M. and Borg L. E. (2006) Trace element and  $^{142}\text{Nd}$  systematics in the nakhlite MIL03346 and the orthopyroxenite ALH84001: Implications for the Martian mantle. *Lunar Planet. Sci. XXXVII*, Lunar Planet. Inst., Houston, #2045(abstr.).
- Wadhwa M. (2001) Redox state of Mars' upper mantle and crust from Eu anomalies in shergottite pyroxene. *Science* **292**, 1527–1530.
- Walker R. J. (2016) Siderophile Elements in Tracing Planetary Formation and Evolution. *Geochemical Perspectives* **5**(1).
- Walker R. J., Yin Q. Z. and Heck P. H. (2018) Rapid effects of terrestrial alteration on highly siderophile elements in the Sutter's Mill meteorite. *Meteorit. Planet. Sci.* **53**(7), 1500–1506.
- Wang Z. and Becker H. (2017) Chalcophile elements in the martian meteorites indicate a low sulfur content in the martian interior. *Earth Planet. Sci. Lett.* **463**, 56–68.
- Warren P. H. and Kallemeyn G. W. (1996) Siderophile trace elements in ALHA84001, other SNC meteorites and eucrites: evidence of heterogeneity, possibly time-linked, in the mantle of Mars. *Meteor. Planet. Sci.* **31**, 97–105.
- Warren P. H., Kallemeyn G. W. and Kyte F. T. (1999) Origin of planetary cores: evidence from highly siderophile elements in martian meteorites. *Geochimica et Cosmochimica Acta* **63**, 2105–2122.
- Yamashita K., Nakamura N., Imae N., Misawa K. and Kojima H. (2002) Pb isotopic signature of Martian meteorite Yamato 000593 (a preliminary report). *Antarct. Meteorit.* **27**, 180–182.
- Zmolek P., Xu X. P., Jackson T., Thieme M. H. and Trogler W. C. (1999) Large mass independent sulfur isotope fractionations during the photopolymerization of  $\text{I}_2\text{CS}_2$  and  $\text{I}_3\text{CS}_2$ . *J. Phys. Chem. A* **103**, 2477–2480.

Associate editor: James M.D. Day